Atlantic Extreme Wave Events During the Last Four Millennia in the Guadalquivir Estuary, SW Spain

Article *in* Quaternary Research · January 2015

DOI: 10.1016/j.yqres.2014.08.005

CITATIONS
39

READS
1,142

11 authors, including:

Antonio Rodríguez-Ramírez
Universidad de Huelva
99 PUBLICATIONS **1,134** CITATIONS
SEE PROFILE

José Noel Pérez-Asensio
University of Granada
42 PUBLICATIONS **603** CITATIONS
SEE PROFILE

Ana Santos
University of Oviedo
93 PUBLICATIONS **1,219** CITATIONS
SEE PROFILE

Gonzalo Jiménez-Moreno
University of Granada
164 PUBLICATIONS **3,892** CITATIONS
SEE PROFILE

Quaternary Research 83 (2015) 24–40

Contents lists available at ScienceDirect

Quaternary Research

journal homepage: www.elsevier.com/locate/yqres

Atlantic extreme wave events during the last four millennia in the Guadalquivir estuary, SW Spain

Antonio Rodríguez-Ramírez [a,*], José Noel Pérez-Asensio [b], Ana Santos [a], Gonzalo Jiménez-Moreno [c], Juan J.R. Villarías-Robles [d], Eduardo Mayoral [a], Sebastián Celestino-Pérez [e], Enrique Cerrillo-Cuenca [e], José Antonio López-Sáez [f], Ángel León [g], Carmen Contreras [a]

[a] Departamento de Geodinámica y Paleontología, Universidad de Huelva, Campus de Excelencia Internacional del Mar, CEIMAR, Avenida 3 de Marzo, s/n 21007 Huelva, Spain
[b] Earth and Environmental Science Section, University of Geneva, Rue des Maraîchers 13, 1205 Geneva, Switzerland
[c] Departamento de Estratigrafía y Paleontología, Facultad de Ciencias, Universidad de Granada, Avda. Fuentenueva s/n, 18002 Granada, Spain
[d] Instituto de Lengua, Literatura y Antropología, Centro de Ciencias Humanas y Sociales (CCHS), Consejo Superior de Investigaciones Científicas (CSIC), C/ Albasanz, 26-28, 28037 Madrid, Spain
[e] Instituto de Arqueología de Mérida, Consejo Superior de Investigaciones Científicas (CSIC), Plaza de España 15, 06800 Mérida, Spain
[f] Instituto de Historia, Centro de Ciencias Humanas y Sociales (CCHS), Consejo Superior de Investigaciones Científicas (CSIC), Calle Albasanz, 26-28, 28037 Madrid, Spain
[g] Fundación del Hogar del Empleado (FUHEM), Colegio Lourdes, C/ San Roberto, 8, 28011 Madrid, Spain

ARTICLE INFO

Article history:
Received 3 February 2014
Available online 12 September 2014

Keywords:
Extreme wave events
Tsunami
Geomorphology
Sedimentary infillings
Holocene
Guadalquivir estuary
Southwest Spain

ABSTRACT

A multidisciplinary study from a number of drilled cores in the Guadalquivir estuary has made possible to identify as many as three extreme wave events and their facies in the 4th millennium BP (A: ~4000 cal yr BP, B: ~3550 cal yr BP, and C: ~3150 cal yr BP). These events, which caused strong erosion in the Guadalquivir sandy barrier and in the neighboring aeolian systems of El Abalario, brought about significant paleogeographical changes that may have affected human settlements established in the area during the Neolithic and Copper Age periods and during the Middle Bronze Age. The three events can be spatially correlated and their facies differentiated from more proximal to more distal from the coastline. The most proximal facies is characterized by a massive accumulation of shells, a sandy or sandy–muddy matrix, an erosive base, a highly diverse mixture of species (marine and estuarine), and lithoclasts. The most distal facies presents a muddy–sandy matrix, dominance of estuarine fauna, shell accumulation, presence of terrestrial species, mudpebbles, pebbles in a clayey matrix, and bioturbation. The evidence presented will further advance scientific knowledge about the impact of extreme wave events on coastal areas in SW Iberia and NW Africa.

Introduction

The impact of extreme wave events can create a complex sedimentary record that has significant morphological effects and drastic ecological impacts in low-energy coastal environments (Bondevik et al., 1997; Dawson and Smith, 2000; Sawai, 2002). Tsunamis and coastal storms are two of the most dangerous and yet most common extreme wave events that affect coastal locations (Morton et al., 2011). These high-energy events cause the deposition of sedimentary beds that have certain specific sedimentological and paleontological characteristics (Fujiwara et al., 2000; Goff et al., 2012).

It is difficult to distinguish tsunamis from severe storms in coastal sedimentary records insofar as both tsunamis and severe storms are high-energy marine events that generate very similar deposits. Many studies have tried to identify diagnostic criteria to differentiate between the two types of events (Fujiwara et al., 2000; Nanayama et al., 2000; Goff et al., 2004; Morton et al., 2007; Goff et al., 2012; Ramírez-Herrera et al., 2012). Because both tsunamis and severe storms impinge violently on the coast and result in the inundation of extensive areas by seawater, both have been referred to as "Extreme Wave Events" or EWEs (Kortekaas and Dawson, 2007; Bridge, 2008; Switzer, 2008; Switzer and Jones, 2008; Lario et al., 2010). Yet it is essential to distinguish between tsunami and storm deposits in sedimentary records, if only because paleo-event analyses are used to predict event recurrence and to conduct hazard vulnerability assessments. Establishing such a distinction is not an easy task, however; numerous multiproxy data, to be found widely distributed in a study area, are needed for such purpose.

Geomorphological and sedimentological features generated by EWEs are well known along the coasts of SW Iberia. Such events have been attributed to tsunamis and/or storm surges (Lario et al., 2010). At present, strong storms occur in the Gulf of Cadiz with a cyclicity regulated by the North Atlantic Oscillation (NAO; periodicity of ~6 yr) as well as by solar irradiation (sunspot cycles) (periodicity of ~11 yr) (Rodríguez-Ramírez et al., 2003). Tsunamis affecting the Gulf of Cadiz have drawn increasing interest since the recent devastating tsunamis in Indonesia, Thailand, and Japan. The received literature registers as

* Corresponding author. Fax: +34 958219440.
E-mail address: arodri@uhu.es (A. Rodríguez-Ramírez).

http://dx.doi.org/10.1016/j.yqres.2014.08.005
0033-5894/

many as sixteen tsunamis hitting the coasts of the Gulf of Cadiz between 218 BC and AD 1900 (Galbis Rodríguez, 1932–1940; Campos, 1992; Bermúdez and Peinado, 2005). Traces of some of these events in the sedimentary record have been sought over the past few decades (Andrade, 1992; Andrade et al., 1994; Lario et al., 1995; Dawson et al., 1996; Dabrio et al., 1999; Luque et al., 2002; Whelan and Kelletat, 2003; Alonso et al., 2004; Gracia et al., 2006; Morales et al., 2008; Baptista and Miranda, 2009; Gutiérrez-Mas et al., 2009; Morales et al., 2011). The epicenters of the corresponding earthquakes have traditionally been placed some 200 km southwest of Cape São Vicente, near the Gorringe Bank (Martínez Solares et al., 1979), yet current analyses point to movements along the Azores-Gibraltar Fault or along associated minor faults such as the Marques de Pombal Fault (Baptista et al., 1998; Terrinha et al., 2003). Historically, the most recent one occurred on November 1, 1755: the notorious "Lisbon earthquake." The tsunami impacted on coastal areas of the Iberian Peninsula and Morocco (Levret, 1991; Scheffers and Kelletat, 2005; Whelan and Kelletat, 2005; Gracia et al., 2006), its effects reaching as far as the south coast of England (Foster et al., 1991).

The interested reader will find in today's geological literature a reference to at least eight EWEs impacting on the SW Iberian Peninsula over the past seven thousand years: ~7000–6800 cal yr BP, ~5700–5300 cal yr BP, ~4500–4100 cal yr BP, ~3900–3700 cal yr BP, ~2700–2200 cal yr BP, ~2200–2000 cal yr BP, ~1500 cal yr BP, and AD 1755 (Lario et al., 2010, 2011; Morales et al., 2011). Comparing the onshore with the offshore records of earthquake-related turbidite deposits (Gràcia et al., 2010) has reduced this number to five tsunamis in the same time span (Lario et al., 2011), within calibrated ages of ~7000–6800 cal yr BP, ~5500–5000 cal yr BP, ~3900–3600 cal yr BP, ~2200–2000 cal yr BP, and AD 1755.

The first, indirect evidence of formations generated by EWEs in the Guadalquivir estuary are chenier deposits and small spits that have formed in the mudflat salt marshes of the estuary (Rodríguez-Ramírez et al., 1996; Ruiz et al., 2005b; Rodríguez-Ramírez and Yáñez, 2008). Additional, more direct evidence comes from sedimentary analysis of sediment cores (Lario et al., 2001; Pozo et al., 2010). Yet a number of factors in the dynamics of the Guadalquivir estuary must be taken into account in attempting to understand its geomorphic evolution, as these factors greatly alter the potential evidence procured from the analysis. In its initial phases before being completely filled, the estuary was a rather large internal lagoon (Rodríguez-Ramírez et al., 1996). Intense tidal and fluvial currents as well as wave movement in the estuary disturbed sediments supplied by EWEs by recycling, mixing, and depositing these sediments in the form of cheniers over fluvial levees (Rodríguez-Ramírez and Yáñez, 2008). These cheniers extend over the surface of the present-day salt marshes and are also buried in the soil. Notwithstanding such complex geomorphic evolution several attempts have been made to establish sequences of tsunamigenic events in the area. Because the nature and dynamics of cheniers were not considered in such attempts, serious mistakes of interpretation have resulted in the scientific literature (Rodríguez-Ramírez, 2009). The only way to secure an analysis of an undisturbed sedimentary record in the lower Guadalquivir marshland is to perform numerous boreholes which will allow having a wide spatial and morphosedimentary view of the sediments along the geography of the old Guadalquivir estuary. Once this is done, the origin of these sediments can be specified.

The main objective of this paper is to document the sedimentary record of EWEs in the lower Guadalquivir marshes over the past 4 millennia and to correlate this record with regional events in the Atlantic Ocean. The evidence presented is the result of a multidisciplinary study of geomorphological, sedimentological, paleontological, chronological, and mineralogical data obtained from fifteen deep and superficial drilled cores which reveal shell-rich and sand facies. Spatially correlated, these drilled cores show the extent and variation of morphosedimentary characteristics of EWEs. This is the first sucessful study on this subject in the Gulf of Cadiz.

Geographical and morphodynamic setting

Located in the central sector of the Gulf of Cadiz, the Guadalquivir estuary is under the influence of the Atlantic Ocean (Fig. 1). It is today enclosed by two spits, Doñana and La Algaida, behind which is a large freshwater marshland of 180,000 ha which includes Doñana National Park, a UNESCOMAB Biosphere Reserve. The estuary comprises the most extensive spit system of the Gulf of Cadiz, which has grown toward the E and SE. At present the spits are partly covered by active dunes. The present freshwater marshes have their origin in the clay contributions of the Guadalquivir and other rivers, which filled the marine estuary in the form of a low-energy finger delta. Growth of the large spits favored this infilling, as they isolated the estuary from the ocean (Rodríguez-Ramírez et al., 1996). There is thus a direct relationship between the littoral and the estuarine formations. With a modest topographic gradient, the freshwater marshes include various muddy and sandy facies which are the byproduct of intense fluvial and marine action.

Hydrodynamic processes in the estuary are controlled by the fluvial regime, the tidal flux, wave action, and drift currents. The largest river draining the Spanish southwest and the main source of fluvial sediments in the entire southwestern coastline, the Guadalquivir has a mean 164 m^3/s annual discharge, even though winter spates can easily exceed 5000 m^3/s (Vanney, 1970). The highest runoff (>1000 $m^3\ s^{-1}$) takes place from January to February, with fluvial current velocities of up to 1 m/s (Vanney, 1970; Menanteau, 1979). The maximum tidal range at the river mouth is 3.86 m (period 1992–2006), with an average of 3.65 m (Spanish Ministry of Public Works). The tidal regime can be described as semidiurnal mesotidal (Borrego et al., 1993).

The wave regime depends directly on the prevailing SW winds, with 22.5% of the days per year in this direction (data of the Instituto Nacional de Meteorología for the city of Huelva: 1960–1990). In the wintertime Atlantic cyclones are common, giving rise to strong SW winds which generate "sea-type" waves more than 6–8 m high (Hsmax; data from Clima Marítimo (OAPE)). These waves cause significant shore erosion, but represent only around 3–5% of the total annual waves. In general, the wave regime in the Gulf of Cadiz is medium-to low-energy, with waves usually smaller than 0.6 m high. Most of the wave fronts approach the coast obliquely and induce littoral currents that transport sand from the Portuguese coast to the Spanish nearshore zone (Cuena, 1991).

Materials and methods

Geomorphology

Aerial photographs from 1956 (1:33,000) and 2010 (1:10,000) were analyzed by photointerpretation to map the detailed geomorphology of coastal sediment bodies. The analysis was complemented by direct observations in the field. The Topographic Map of Andalucia (1:10,000) was used as a base document for geomorphological mapping. All of this information was integrated and analyzed into the gvSIG GIS program.

Lithostratigraphy

It was examined the sedimentary sequence obtained from two boreholes 12 m deep (S7 and S9) and from one borehole 18 m deep (S11). The drilling took place between 2006 and 2009 as part of a multi-institutional research project of regional scope named "The Hinojos Project." The drilling was done by a direct circulation rotary method, with continuous core sampling (Cruse, 1979). Point S9 was placed relatively close to S7 in order to verify the lateral continuity of the sedimentary formations; detailed analyses were only made for S7 and S11 (Fig. 2). Other cores examined were those drilled at points PN and ML, previously studied by Pozo et al. (2010) and Zazo et al. (1999). In addition the present research studied the sediments from a number of shallow drillings (<3 m) in surface formations on both banks of the Guadalquivir River (CV1, CV2, CV3, M1,

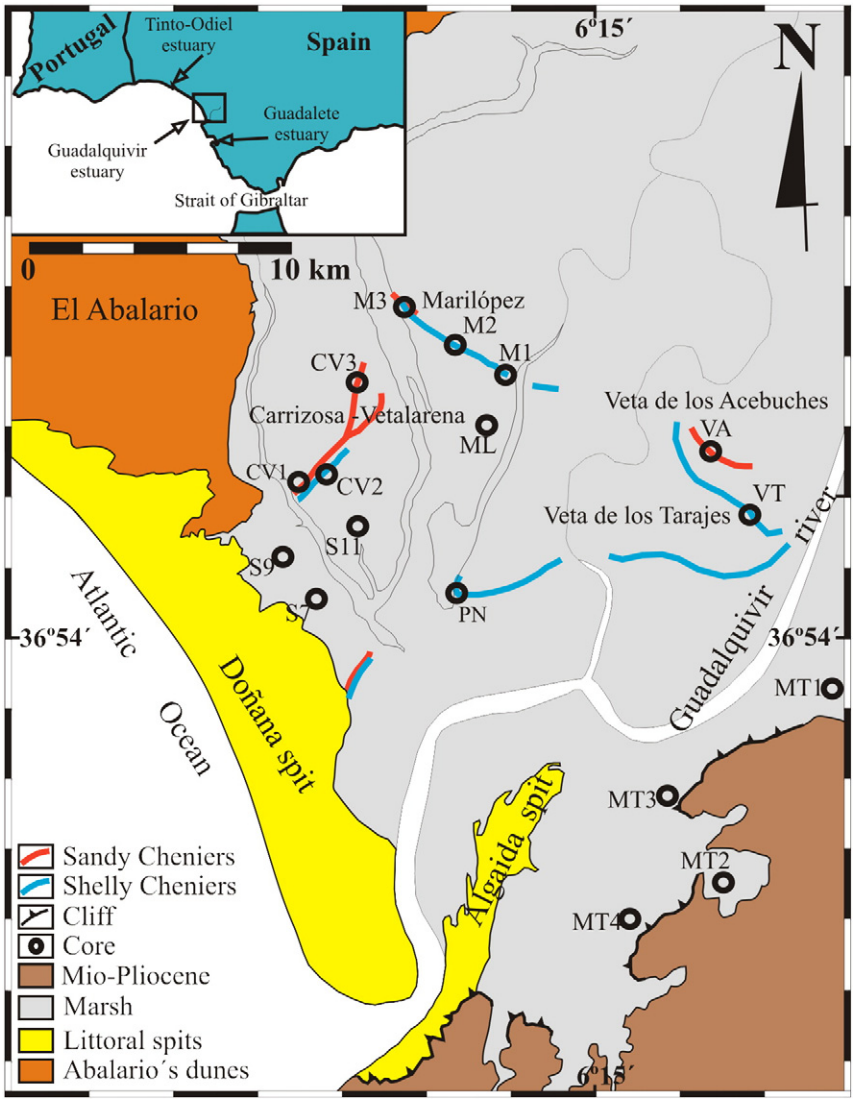

Figure 1. Study area and location of cores. ML and PN from Zazo et al. (1999) and Pozo et al. (2010), respectively.

M2, M3, VA, VT, MT1, MT2, MT3, and MT4) (Fig. 1), for which it was used a 2-cm diameter Eijkelkamp gouge and an 8-cm diameter helicoidal drill.

The main focus of interest was the sandy levels found interbedded in the thick clay sediments of the marshland, specifically the morphology, geometry, and extension of these sandy levels and their relationship with underlying and overlying sediments. The stratigraphy and lithology of each recovered core were described in the field. Grain-size distribution was determined in the laboratory by wet sieving for the coarser fractions (>100 μm small) and by photosedimentation on a Mastersizer 2000 laser diffractometer ("Sedigraph 5100") for fractions smaller than 100 μm.

Paleontology

Macrofossil analysis from sediment samples was undertaken in order to identify species type and diversity (faunal composition and shell preservation). Thirty-three samples were collected from different cores (S11, S7, VA, VT, MT3, and MT1) and prepared by washing the bulk sediment (12 cm^3) through a 1 mm sieve. Bivalves and gastropods were identified to the species level and then counted to study the semi-quantitative distribution of species in each core. The presence and relative abundance of other groups (such as scaphopods, barnacles, and bryozoans) were also noted (Figs. 4, 5).

Cores S7 and S11 were analyzed for foraminiferal content (Fig. 3). Twenty-one samples of 50 g each were taken and analyzed from core S7. The sampling interval was 0.5 m from 0 to −9 m and 1 m from −9 to −12 m. Thirty-six samples of 50 g each were taken and analyzed from core S11; the sampling interval was here 0.5 m throughout. Foraminiferal analysis was also performed on 13 samples collected from the short cores drilled in surface formations. The samples were washed over a 63 μm mesh, oven-dried at 40°C, and weighed. A microsplitter was used to obtain sub-samples containing at least 300 benthic foraminifera. In the size fraction >125 μm, benthic foraminifera were identified to the species level and counted; these counts were then transformed into relative abundances. Q-mode principal component analyses (PCA) were conducted in order to obtain the benthic foraminiferal assemblages; IBM SPSS Statistics 20 was used (Table 1). Only species with a relative abundance ≥0.5% in at least 3 samples were considered. In order to assess the marine influence in the estuary, the percentages of total, porcelanaceous, and hyaline transported benthic foraminifera were calculated. Finally, the planktonic/benthic ratio (P/B ratio henceforth), scored as [P/(P + B) × 100], was also employed for determining sea-level changes or marine influence.

Cores S7 and S11 were also subjected to pollen and dinoflagellate cyst (dinocyst) analysis, with a sampling interval at 0.5 m (42 samples) using 2 cm^3 of sediment. The dinocyst/pollen ratio (d/p ratio hereafter), scored as [d − p]/[d + p], was used as a proxy for assessing sea-level changes or marine influence (Fig. 3).

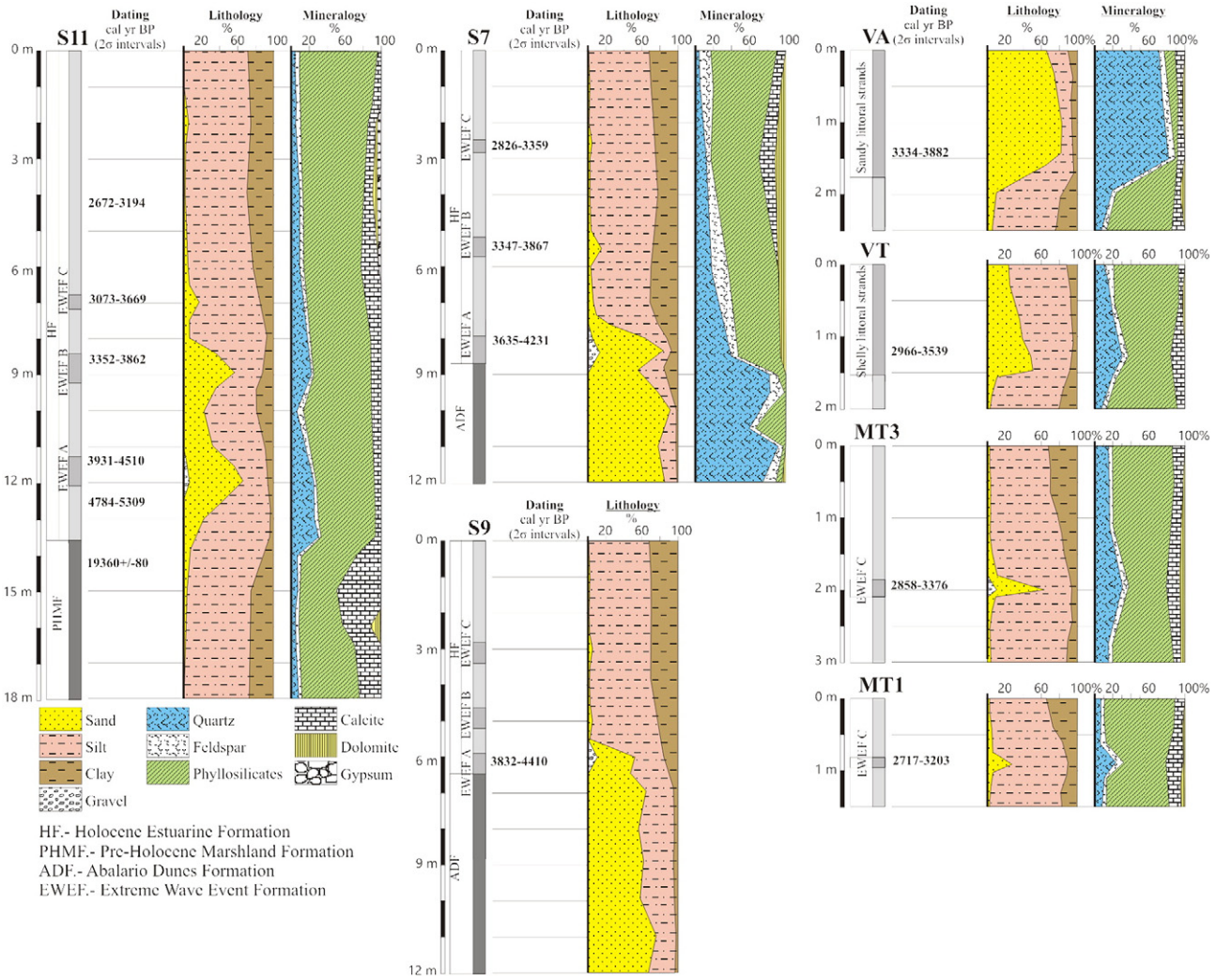

Figure 2. Lithostratigraphy, mineralogy, and chronology of the cores S7, S9, S11, VA, VT, MT3, and MT1.

Mineralogy

Mineralogical analyses, carried out in laboratories of the University of Huelva, were conducted by powder X-ray diffraction (XRD) techniques on a Bruker-AXS D8-Advance diffractometer, using monochromatic CuKα radiation at 40 kV and 30 mA. Random powders were scanned from 3 to 65° 2θ at 2° 2θ/min, after gentle grinding and homogenization to <63 μm.

Dating

Fifteen radiocarbon dates were obtained with the AMS method applied to mollusc shells in the facilities of Beta Analytic Laboratory (Florida, USA), Centro Nacional de Aceleradores (Seville, Spain), and Accium BioSciences Accelerator Mass Spectrometry Lab (Seattle, USA) (Table 2). The shells selected were those that showed, wherever possible, no transportation or low degree of transport, and were preserved as articulated valves in the lag deposit. Additional published radiocarbon data were also used (Rodríguez-Ramírez et al., 1996; Zazo et al., 1999; Ruiz et al., 2005b; Pozo et al., 2010). Radiocarbon ages were calibrated by using CALIB 7.0 (Stuiver and Reimer, 1993) as well as the Stuivert et al. (1998) calibration dataset. The final results correspond to calibrated ages (cal) with 2–σ intervals, corrected for the reservoir effect with the parameter suggested by Soares and Martins (2010) for the Gulf of Cadiz (Table 2 and Fig. 7). For the Late Holocene on the Andalusian coast of the Gulf of Cadiz, Soares and Martins (2010) recommended a ΔR value of -135 ± 20 ^{14}C yr; except for the range 4400–4000 ^{14}C yr BP, for which he suggested a value of $+100 \pm 100$ ^{14}C yr. Lack of sufficient data for the years 4000–2000 ^{14}C yr BP preclude determining with enough assurance the most recent time boundary to which the $+100 \pm 100$ ^{14}C yr ΔR value can be extended. We chose to extend it to the middle year 3000 ^{14}C yr BP. New data on reservoir effects are necessary to calibrate with greater precision samples from the Gulf of Cadiz.

The resultant isotopic determinations were compared with the age of archeological remains known from the area (Menanteau, 1979). In addition, pottery sherds were discovered in and extracted from the littoral strands of Carrizosa–Vetalarena (CV1); they were sent to Instituto de Arqueología del CSIC (in Mérida, Spain) for typological analysis and dating.

Results

Geomorphology

The marshland is geomorphologically characterized by fluvial levees flanking the Guadalquivir River and its ancient courses. These clay-rich levees have a variable width (300–2000 m) and great length; in addition, they reach heights of 0.5–1.8 m above the adjacent interlevee marshes, where the most flooded zones are located.

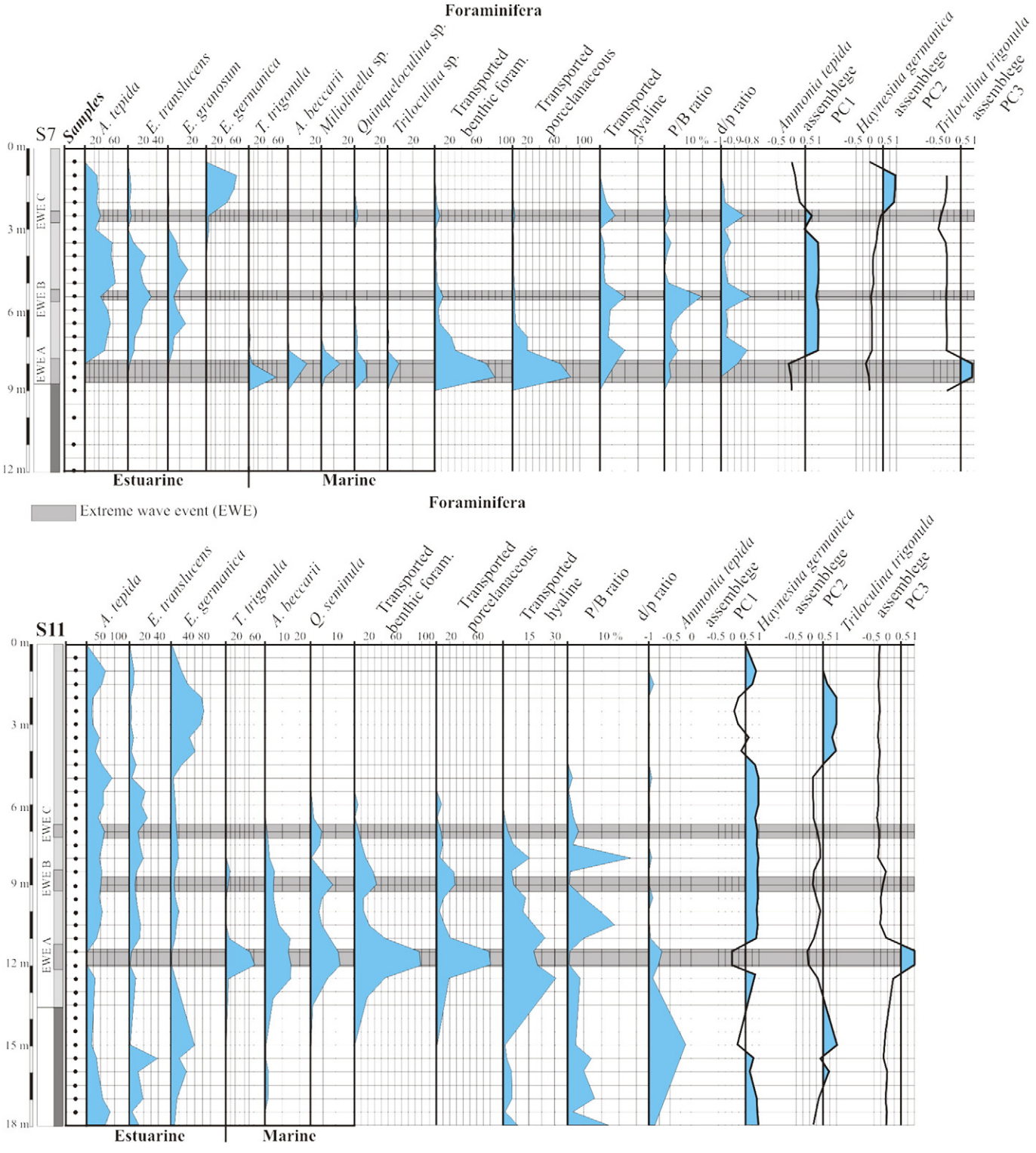

Figure 3. Micropaleontology of cores S7 and S11.

On the river right bank, overlying the marsh clay deposits, stands a series of sandy and shelly formations with littoral strand morphology. These formations are part of a wider chenier plain, which extends toward the north and is being eroded by agricultural activities. The cheniers lie on the south-western bank of the different fluvial levees of the marshland; they have beach ridge morphology, with narrow and small ridges and landward-dipping crests. No littoral strand morphologies exist on the left bank of the Guadalquivir River.

The dune systems of El Abalario extend to the north and west of the marshland, reaching heights of over 100 m above sea level. Geomorphologically, as many as five semi-stable dune systems, moving in NW and W directions, can be distinguished. These aeolian units began to accumulate ~5 cal ka BP (Zazo et al., 2008), the oldest units lying deeper than the marshland sedimentary formations. Prehistoric artifacts from the Neolithic period and the Copper Age (~6000–4000 ^{14}C yr BP) have been found widely dispersed among the dunes (Campos and

Table 1
S7 and S11 Q-mode PCA results with indication of the explained variance (%) of each PC axis (assemblage) and the dominant and most significant associated species.

PC	Variance (%)	Species	Score
S7			
1	57.6	*Ammonia tepida*	4.74
		Elphidium translucens	1.45
		Elphidium granosum	0.57
2	20.9	*Haynesina germanica*	4.93
		Ammonia tepida	1.19
3	10.9	*Triloculina trigonula*	4.02
		Ammonia beccarii	1.59
		Miliolinella sp.	1.37
		Quinqueloculina sp.	0.99
		Triloculina sp.	0.70
S11			
1	62.3	*Ammonia tepida*	4.90
		Elphidium translucens	1.07
2	27.0	*Haynesina germanica*	5.05
		Ammonia tepida	0.46
3	6.9	*Triloculina trigonula*	4.67
		Ammonia beccarii	1.25
		Quinqueloculina seminula	0.99

Gómez-Toscano, 1997). The boundary to the south of the marshland is constituted by Miocene and Pliocene sediments in the form of hilly reliefs around 70–80 m high in which fossil cliffs have developed.

Lithostratigraphical, paleontological, and mineralogical analysis of the deep cores: S7, S9, and S11

Aeolian sands facies (El Abalario Dune Formation, ADF)

Cores S9 and S7 revealed a similar stratigraphic sequence. The lower portion of both cores – from −12 to −6.5 m and from −12 to −8.5 m, respectively – consists of a sequence of fine to medium sands (75–90% sand, 5–20% silts, 1–4% clay), well sorted (≈65–70% around 0.125–0.5 mm), white-orangish (10YR7/8) in color, and containing abundant red stains, roots, and bioturbation (Fig. 2). Both macro- and microfauna are absent.

Pre-Holocene Marshland Formation facies (PHMF)

These facies appear at the lower part of core S11 (Fig. 2), from −18 to −13.5 m. It is a sequence of mostly clayey silts (70–75% silts, 20–25% clay, 2–5% sand) of a grayish ochre (10YR8/2) color, with burrow, roots, carbonate nodules, oxidation, and intense lamination. Detrital minerals are present with a proportion of 6–10% quartz and 2–4% feldspar. Calcite varies from 15 to 35%, phyllosilicates from 50 to 70%, dolomite with 7%. The macrofauna is absent and the foraminifera are dominated by an *Ammonia tepida* assemblage (PC1: Estuarine) in the lower part of the facies, with *Elphidium translucens* as secondary species. A *Haynesina germanica* assemblage (PC2: Estuarine), with *A. tepida* as associated species, dominates in the upper part (Fig. 3).

Clayey silts facies

The lithology dominant in all cores is a gray-greenish (10YR6/1) clayey silt: 50–60% silt, 15–35% clay, 10–1% sand, with more ochre tones (10YR6/4) in the upper 2 m. The lower part of S11 presents the largest amounts of sand content (20–30% sand), from −13.5 to −7.5 m, turning progressively into clayey silts toward the top (<1% sand). Regarding mineralogy, the detrital component shows an upward decrease in quartz and feldspar: from 40% and 20% to 5% and 2%, respectively. Phyllosilicates exhibit increase toward the top of 80–90%. Calcite and dolomite values are between 10–40% and 10–14%, with a maximum at −3 m below surface and diminishing toward the top.

The micropaleontological analysis revealed in the lower and middle parts of this facies an *A. tepida* assemblage (PC1: Estuarine), which includes *Elphidium translucens* and *E. granosum* as associated taxa; they are typical of brackish estuarine environments (Ruiz et al., 2005a; Murray, 2006; Pérez-Asensio and Aguirre, 2010). In the upper part, another estuarine assemblage, dominated by *H. germanica* (PC2: Estuarine) with *A. tepida* as accompanying species, is significant. The values of transported benthic and porcelanaceous foraminifera are low. In S7 and in the upper part of S11, from −7.5 m to the top, the transported hyaline foraminifera, the P/B ratio, and the d/p ratio revealed similar trends. In the lower part of core S11, of more sand content (from −13.5 to −7.5 m), the transported hyaline foraminifera reach significant values. The highest values of the P/B ratio are found at 10.5 and 8 m. The d/p ratio presents a very low value (Fig. 3).

Table 2
Data base of ^{14}C results using the Marine04 curve (Hughen et al., 2004), the program CALIB rev. 6.0 (Stuiver and Reimer, 1993) and ΔR suggested by Soares and Martins (2010). B. — Beta Analytic Laboratory (Miami, USA). CNA. — Centro Nacional de Aceleradores (Seville, Spain). DAMS. — Accium BioSciences Accelerator Mass Spectrometry Lab (Seattle, USA). CX. — Geochron Laboratories, Krueger Enterprises, Inc., (Cambridge, USA). (1) Rodríguez-Ramírez et al. (1996). (2) Ruiz et al. (2005b). (3) Pozo et al. (2010). (4) Zazo et al. (1999).

Core	Depth	Lab. ref.	^{14}C yr BP	$\delta^{13}C$‰	^{14}C cal yr BP (2σ intervals)	ΔR (^{14}C yr)
S7	−2.5 m	B-285000	3370 ± 40	0.1	2826–3359	100 ± 100
S7	−5.5 m	B-285001	3780 ± 40	0.4	3347–3867	100 ± 100
S7	−8 m	B-285002	4040 ± 40	1.3	3635–4231	100 ± 100
S9	−6 m	B-285004	4180 ± 40	0.6	3832–4410	100 ± 100
S11	−4 m	B-285006	3190 ± 40	−2.5	2672–3194	100 ± 100
S11	−7 m	D-AMS 002422	3596 ± 60	−4.6	3073–3669	100 ± 100
S11	−8.5 m	D-AMS 001537	3781 ± 33	5.5	3352–3862	100 ± 100
S11	−11.5 m	D-AMS 001538	4260 ± 30	2.9	3931–4510	100 ± 100
S11	−12.5 m	B-285007	4860 ± 40	−0.3	5255–5461	−135 ± 20
S11	−13.5 m	B-285008	19360 ± 80	−25.2	Uncalibrated	
PN	−10.8 m	B-228881 (3)	4060 ± 40	–	3665–4269	100 ± 100
ML	−7.3 m	CX-238339 (4)	3915 ± 50	−1.9	3473–4066	100 ± 100
VT	−1.1 m	CNA1117	3504 ± 48	−6.9	2966–3539	100 ± 100
VA	−1.5 m	D-AMS-002424	3778 ± 54	1.0	3334–3882	100 ± 100
MT3	−2 m	D-AMS-1217-180	3398 ± 27	3.8	2858–3376	100 ± 100
MT1	−1 m	D-AMS-1217-179	3233 ± 26	−1.7	2717–3203	100 ± 100
CV1	−0.5 m	B-287646	4370 ± 40	−1.8	4071–4706	100 ± 100
CV2	−0.4 m	B-154084 (2)	3380 ± 40	−0.8	2835–3369	100 ± 100
M3	−0.5 m	B-154087 (2)	3460 ± 40	−1.6	2916–3464	100 ± 100
M3	−1.3 m	B-154085 (2)	4260 ± 40	−1.9	3922–4514	100 ± 100
M2	−0.70 m	R-2279 (1)	3679 ± 48	–	3210–3766	100 ± 100
M1	−0.60 m	R-2280 (1)	3694 ± 61	–	3227–3808	100 ± 100

The macrofauna in the clayey-silty facies appeared to be dominated by shallow-water estuarine fauna from sheltered environments, including *Tellina tenuis*, *Abra abra*, *Cerastoderma edule*, *Saccostrea virletii*, and *Nassarius* sp. In general, these bivalve shells indicate a low degree of transport: both valves were present and some of them even in life position. Open marine species – *Nucula* (*Nucula*) *nitidosa*, and *Bittium reticulatum* – were very sparse and found scattered, having been transported to the studied area. From −2 m to surface very few fragments of *Cerastoderma edule* were found (Fig. 4).

EWE facies

Different decimetric layers with a higher sand content appeared in the cores (Figs. 2, 3, 4).

EWE A. The first sand layer consists of gray-yellowish (2.5Y7/3) heterometric sands, the S7 core yielding fine- to coarse-grained, poorly sorted sands (80–90%), along with pebbles (5 × 5 cm) and gravel, as well as plant remains (wood). The S11 core produced a lesser amount of sand (55–65%) with gravel and pebbles, within a matrix containing a relatively high percentage of sandy silt and some bioturbation. In S7 the bottom is strongly erosive, while in S11 it is only slightly so. S7 presents the sand deposit as a massive sequence, and S11 as a moderate, fining-upward one. The thickness is 0.7 m in S7 (−7.8 to −8.5 m) and 0.5 m in S11 (−11.5 to −12 m). Mineralogical analyses revealed 40% quartz, 6–7% feldspar, 10% dolomite, and 40–45% phyllosilicates (Fig. 2).

The micropaleontological analysis (Fig. 3) revealed that the *Triloculina trigonula* assemblage (PC3: Marine) – with *Ammonia beccarii*, *Miliolinella* sp., *Quinqueloculina seminula*, *Quinqueloculina* sp., and *Triloculina* sp. as secondary taxa – is very important in this sand layer. This assemblage includes shallow water marine species (González-Regalado et al., 2001; Mendes et al., 2004; Ruiz et al., 2005a). Transported foraminifera (benthic, porcelanaceous and hyaline) were very abundant. The d/p ratio has a maximum and the P/B ratio present a low value. The macrofauna, with a high diversity of species (Fig. 4), is composed of a mixture of articulated/disarticulated bivalves shells and fragments. Open marine species were dominant in this mixture. In general for the EWE facies (A, B, and C), while the marine species were transported to this area and worn out, the estuarine bivalve species were found well preserved with articulated valves. The more abundant marine species were *Glycymeris* sp., *Chlamys* sp., *Acanthocardia* sp., *Anomia ephippium*, *Bittium reticulatum*, and *Megastomia conspicua*, as well as corals, scaphopoda, and spines of echinoderms. The more abundant estuarine species were *Cerastoderma edule*, *Tellina tenuis*, *Saccostrea* sp, and *Nassarius* sp.

EWE B. The second sand layer appeared in S7 at −5.5 m (10 cm; 15–20% sand), with a fining-upward succession, its boundary with the lower formation of clayey silts being slightly erosive. In S11 this second peak in the sand component (60% sand) registers at −9 m, within a 25 cm layer that has normal grading and an erosive boundary with regard to the lower sequence.

The micropaleontological analysis revealed (Fig. 3) that the PC2 assemblage dominates this sand layer. Transported foraminifera (benthic, porcelanaceous, and hyaline) were relatively few compared to event A. In core S7 the d/p ratio and the P/B ratio has a maximum. In core S11 this parameter has a low value. The macrofauna (Fig. 4) revealed an increase in fossil remains of estuarine bivalve species, both as articulated as disarticulated valves.

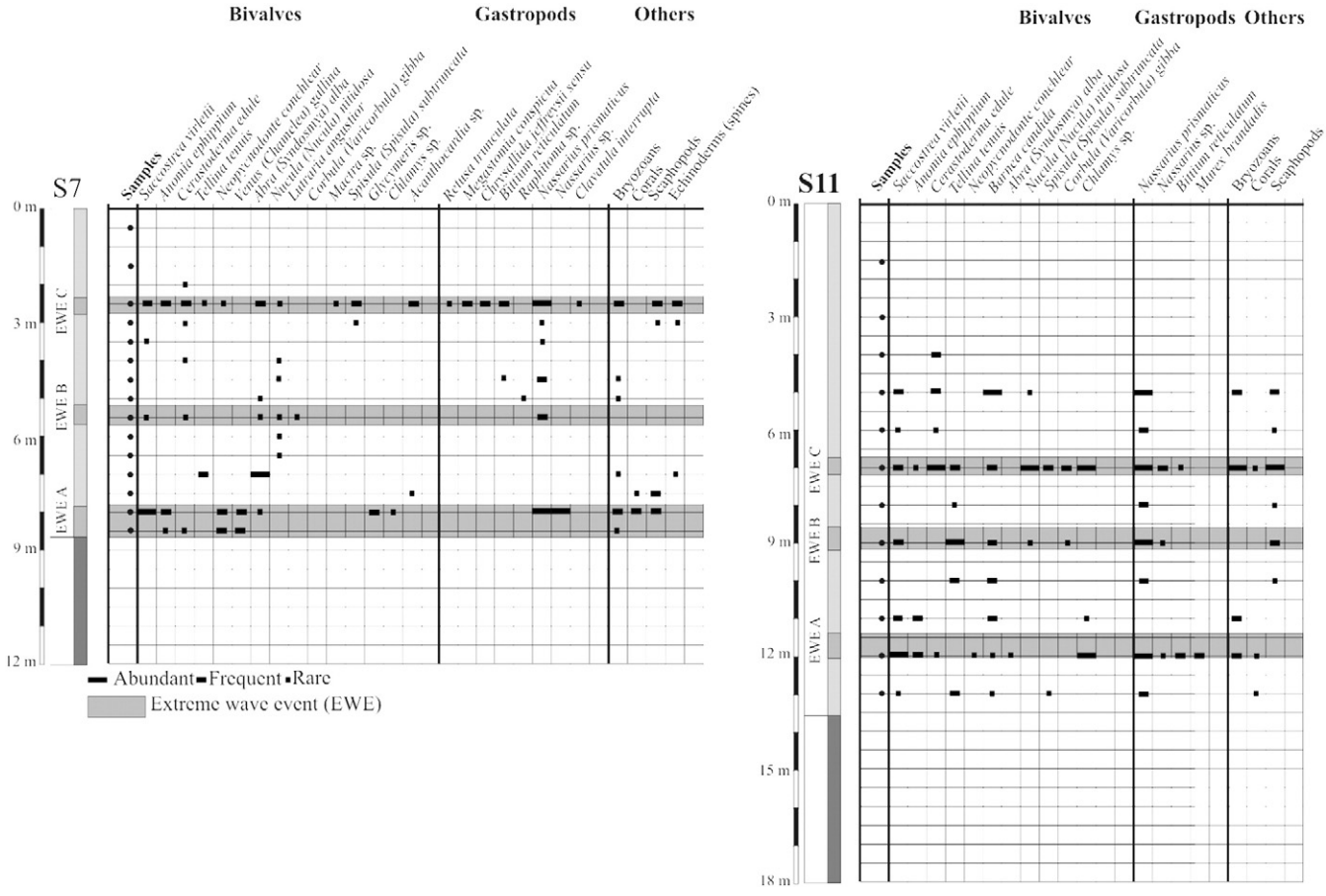

Figure 4. Macropaleontology of cores S7 and S11.

EWE C. In S7 the third level (also 10 cm) was found at −2.5 m (3–7% sand), being more massive than and presenting an erosive base with regard to the underlying silty formation. Some scattered small pebbles appeared in these layers. In S11, a third rise in sand content (up to 15–20%) emerged at −7 m, within 10 cm of sandy silts in a fining-upward sequence on an erosive base, with presence of scattered small pebbles and mud pebbles. This sandy level is overlain by another 10 cm-thick sedimentation of slightly sandy silts (5–10% sand) that were very bioturbated, showing vertical burrows of bivalves. Similar facies, in relation to tsunami events, have been registered in the Tinto–Odiel estuary (Morales et al., 2008).

The micropaleontological analysis (Fig. 3) revealed that the PC2 assemblage dominates this sand layer. Transported foraminifera (benthic, porcelanaceous and hyaline) have a very low value. In core S7 the d/p ratio and the P/B ratio has a maximum. In core S11 this parameter has a low value. The macrofauna analysis (Fig. 4) yielded abundant articulated/disarticulated bivalves shells and shell fragments, of high diversity of species typical of marine environments as well as species that are typical of the inner estuary (Fig. 4)

Minor events facies: The uppermost sedimentation in S7 and S11 also includes deposits that may be evidence of other less significant events in the area (at −3.5 m in S7 and at −6, −5, −4, −2, and −1 m in S11). Such events generated no significant changes in the lithological and stratigraphic sequence, only slight increases in the sand content (1–3%) as well as a gradual boundary with the underlying layer and increases in the dinoflagellates/pollen ratio, transported benthic foraminifera, and malacofauna (Fig. 3). The foraminifera are dominated by the PC2 assemblage and the macrofauna (Fig. 4) presented a low species diversity, with some estuarine forms of disarticulated/articulated bivalves.

Lithostratigraphical, paleontological, and mineralogical analysis of the surface cores

Clayey silts facies

Cores MT1 and MT3 have been plotted in Figures 2 and 5 as representative of the set of surface cores drilled on the left bank of Guadalquivir River (MT1, MT2, MT3, and MT4). The general sequence encountered in these four cores includes gray-ochre (10YR8/4) clayey silts (55–70% silts, 20–35% clay, 2–5% sand) with abundant bioturbation and roots. This sequence resembles the facies of the upper part of cores S9, S7, and S11. The detrital component consists of low values of quartz (15–10%) and feldspar (6–3%), which contrasts with the abundant phyllosilicates (80–90%) and 6–10% calcite (Fig. 2).

EWE facies

A layer of quite heterometric massive silty sands appeared at a depth of about −0.8 m in MT1 and of about −1.5 m in MT3. Interbedded between silts, this layer presents an erosional unconformity with the underlying deposits. Its thickness is variable, ranging from 10 to 25 cm. The percentages of detrital minerals in it are 50–70% quartz, 5–17% feldspar, and 20–35% phyllosilicates (Fig. 2). This layer appeared in all four cores. In MT3 and MT4, the sand content appeared to be higher (50–65%) and to include abundant rock fragments of diverse nature and large size (40 × 50 cm) embedded in the sandy muddy matrix. These pebbles derive from calcarenite formations of both the late Pleistocene – known locally as *Ostionera* facies, generated during sea-level highstands – and the Miocene. While *Ostionera* calcarenites outcrop in the present-day Guadalquivir river mouth as a marine abrasion platform, extending some kilometers out to sea, the Miocene calcarenites can be seen in the neighboring sediments of the Neogene. The Miocene calcarenites recognized in MT3 appear in the form of large boulders (1 × 1.5 m).

In MT2 and MT1 the sandy fraction was lower (20–30%). MT2 yielded abundant pottery sherds along with some pillar material for construction that showed evident marks of transport. Toward the northeast pebbles disappear, whereas mud pebbles interbedded in the sedimentary sequence are common. Overlying this sandy layer, more recent sedimentation 5 to 15 cm thick contained very bioturbated slightly sandy silts, with vertical burrows of anelids and bivalves. Some lithoclasts were found in MT2.

Microfaunal analysis revealed significant percentages of transported marine benthic foraminifera and a relatively high P/B ratio in the sand layer of MT3 (Fig. 5). MT1 yielded very low percentages of transported marine benthic foraminifera and a P/B ratio of 23.67%. Most of the transported benthic foraminifera were hyaline in all samples.

Macrofaunal analysis produced, in MT3 and MT4, a rather conspicuous mixture of disarticulated valves and shell fragments of marine bivalves and gastropods accompanied by other estuarine species (Fig. 5), which is a sign of the varied origins of the sediment inputs. The macrofauna in MT3 was highly diverse: from bivalves (*Crassostrea gigas*, *Anomia ephippium*, *Venerupsis decussata*, *Tellina* sp., *Eastonia rugosa*, *Glycymeris glycymeris*, *Cerastoderma edule*, *Solen marginatus*) to gastropods (*Bittium reticulatum*, *Nassarius* sp., *Murex brandaris*) and from scaphopods (*Dentalium* sp.) to bryozoans and corals. MT1 included a massive layer of *Cerastoderma edule* with articulated shells, *Scrobicularia plana*, and other sporadic marine bivalves (*Saccostrea virletii*, *Barnea candida*, *Tellina* sp.), together with a significant amount of terrestrial gastropods (*Cochlicela* sp.). The *Scrobicularia plana* presented vertical burrows starting from the lower shell level and finishing with the shell itself in life position. MT2 comprehended a mixture of marine shells (*Venerupis decussata*, *Tellina* sp.) and estuarine species (*Cerastoderma edule*).

Shelly formations of the chenier plain

The VT sequence has been plotted in Figures 2 and 5 as representative of the sequences encountered on the shelly littoral strands of the chenier plain that extends toward the west of the right bank of the Guadalquivir River (M1, M2, M3, CV2). All of these cores revealed a lower interval characterized by massive, blue-gray (2.5Y8/2) clayey silt (50–70% silts, 50–30% clay, 1–3% sand) containing traces of burrowing organisms, numerous roots, and scattered fragments of *Cardium edule*. The low percentages of quartz (15–10%), feldspar (6–3%), and calcite (6–10%) contrast with the high content of phyllosilicates (80–90%) (Fig. 2).

The upper formation is made up of 0.5–1.5 m thick lenticular lumachel accumulations of invertebrate shells. These accumulations include numerous bioclasts (30–40% dry weight) as well as sporadic rock fragments in a scarce silty–clayey matrix – even though this matrix becomes more developed upwards (48%) – together with soil development and abundant roots. The sand fraction ranges from 30–50% at the base to 10–14% at the top. In M3 (Fig. 1) the lenticular accumulations (over 0.7–1 m thick) include fine to very fine silty sands, very rich in quartz (65–90%), that correspond to the chenier plain sandy formation.

On the surface these accumulations form a long, narrow ridge (10–30 m wide) (Fig. 6). The sediment succession starts with an erosional unconformity with the underlying deposits, the internal structure of which appeared to be characterized by gentle landward-dipping lamination interrupted by large-scale crossbedded sets with minor amounts of mud at the base. This cross lamination progressively disappears landwards, giving way to a fine bed about 10 m long. The sequence, interrupted by several erosive surfaces, shows a number of overlying beds that exhibit the same characteristics, thus highlighting vertical aggradation.

Macrofauna appeared to be strongly dominated, in general, by disarticulated valves of *Cardium edule* accompanied by other marine bivalves which are evidence of the varied origins of the sediment input (Fig. 5). VT presents a large diversity of organisms, comprising bivalves (*Mactra corallina*, *Solen marginatus*, *Cerastoderma edule*, *Abra* sp., *Crassostrea angulata*, *Tellina* sp., *Chlamys* sp., *Flexopecten glaber*, *Barnea candida*, *Venerupsis decussata*), gastropods (*Nassarius incrassata*, *Murex brandaris*, *Ocenebra erinaceus*), scaphopods (*Dentalium* sp.), and

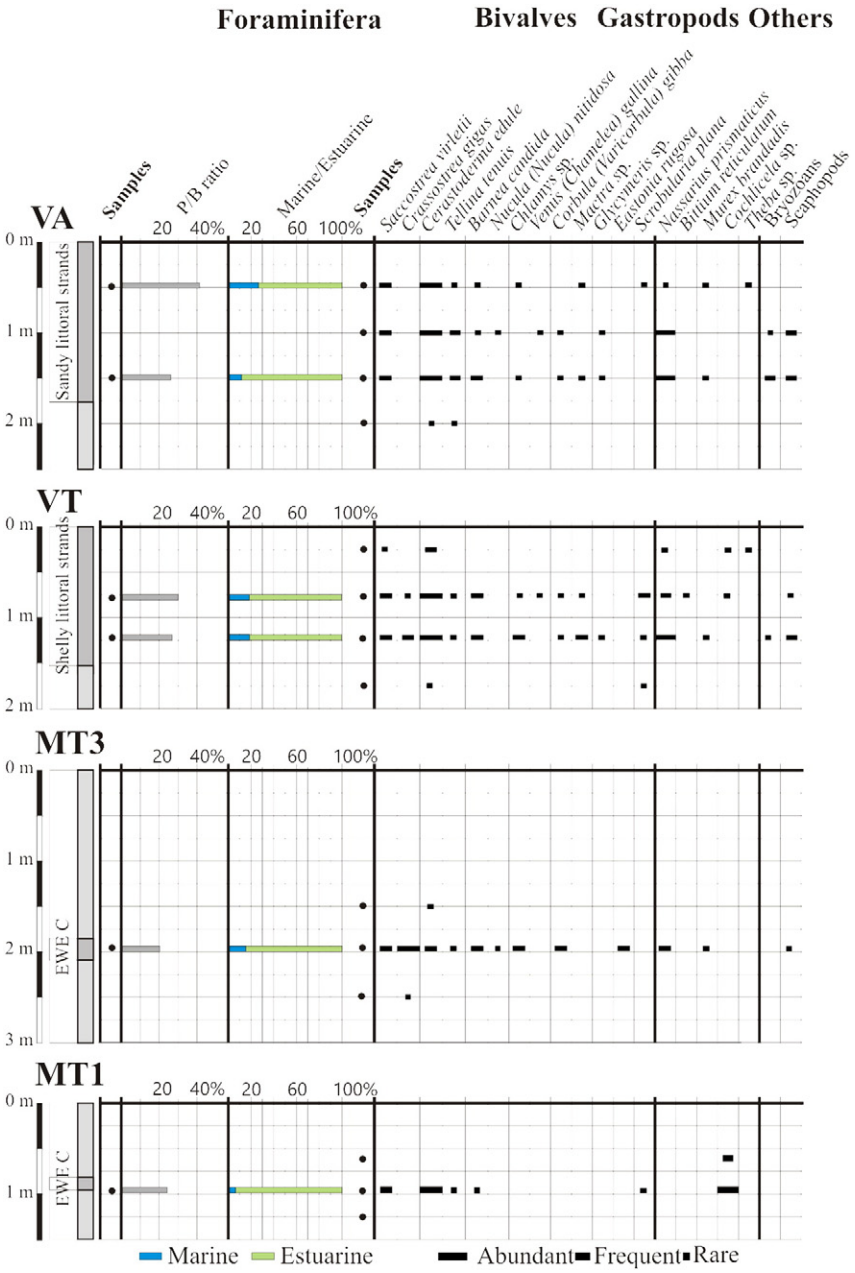

Figure 5. Macropaleontology and micropaleontology of cores VA, VT, MT3, and MT1.

corals. *Cerastoderma edule* is dominant to the west (M1, M2, and M3) where diversity is lower, although other estuarine forms appear (*Crassostrea gigas*, etc.). The foraminiferal content in the accumulations is characterized by very low percentages of transported benthic foraminifera and planktonic foraminifera (Fig. 5). Furthermore, most of the transported benthic foraminifera are hyaline in all samples.

Sandy formations of the chenier plain

The VA sequence is shown in Figure 2 as representative of the cores drilled along the sandy littoral strands of the chenier plain that extends toward the west (Carrizosa–Vetalarena; CV1, CV3) (Fig. 6). These sandy formations present a fine to medium sand rich in quartz (65–90%), with very good sorting and some dispersed pebbles. Feldspar represents 7–12%; calcite, 8–15%; phyllosilicates, 20–35% (Fig. 2). The thickness of the deposit is variable (2.5–1.5 m) and forms a wedge shape that progressively thins landwards. In general, internal structures are scarce and difficult to observe, with subparallel lamination dipping seawardly as well as landwardly; in addition, they are highly bioturbated by vegetation. Subject to erosion, these formations present an unconformable disposition on massive gray clays that contain low percentages of sands (2–8%). At M3 these sandy formations underpin the lenticular accumulations of the shelly cheniers.

The VA core revealed erosive levels with abundant, highly reworked and transported mollusc fauna in which disarticulated valves of *Cardium edule* accompanied by other marine bivalves (*Solen marginatus*, *Glycymeris* sp., *Chlamys* sp., *Donax trunculus*, *Nassarius* sp., *Barnea candida*) predominate. The presence of fauna is poorer to the west (Carrizosa–Vetalarena): only some scattered marine macrofossils (*Crassostrea gigas*, *Glycymeris* sp., *Flexopecten glaber*, *Venerupsis decussatus*, *Venus* (*Chamelea gallina*)) (Fig. 5) were found. Microfaunal analysis of the VA core yielded significant amounts of transported benthic foraminifera as well as relatively high P/B ratios (Fig. 5). At CV1 we discovered an assortment of small pottery sherds from the Neolithic and the Copper Age, highly reworked and transported.

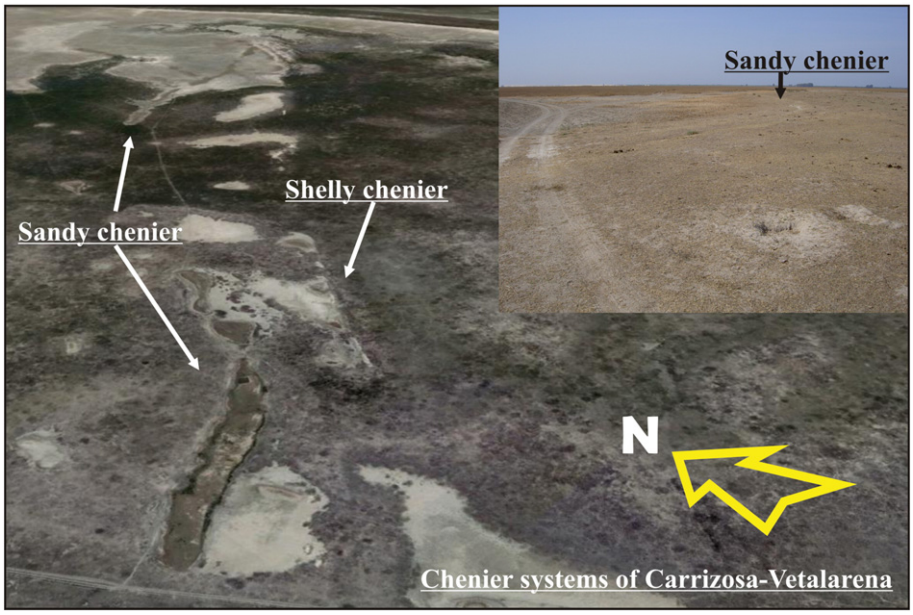

Figure 6. Chenier systems of Carrizosa–Vetalarena from satellite image (year 2012) and fieldwork photograph (year 2010).

Discussion

Pre-Holocene formations

The bottom of some of the analyzed cores (S7, S9, and S11) registers various sedimentary formations that are pre-Holocene in age (PHMF and ADF) (Fig. 2). In S7 and S9 these formations consist of white-yellowish sands without fauna belonging to the aeolian systems that crop out farther north, in the area known as "El Abalario" (Fig. 1). These systems, "El Abalario Dune Formation (ADF)," have been studied at a regional scale both geomorphically and stratigraphically. They reach a considerable thickness and extension on the right bank of the Guadalquivir estuary and make up the substrate for the Holocene formations in the sedimentary infilling of the paleoestuary (Zazo et al., 2005; Salvany et al., 2011). In S11 such pre-Holocene substrate we have named "Pre-Holocene Marshland Formation" (PHMF). Constituted by clayey silts from an ancient floodplain with evident edaphic marks of continentalization, the PHMF has been recognized in all studied cores from the region (Menanteau, 1979; Zazo et al., 1999; Salvany et al., 2011). Radiocarbon dates obtained from the uppermost part of the PHMF are ~20 cal ka BP (Table 2).

The evidence of the Holocene transgressive process

Sea level started to rise after the end of the last glacial period (19 cal ka BP) and has continued to do so ever since (Lambeck et al., 2002). In the estuaries of SW Iberia the present-day level of the Atlantic ocean was reached ~5 cal ka BP, the oscillations recorded since then not exceeding 1 m above and below this mark (Zazo et al., 2008). The first sedimentary evidence of this progressive sea-level rise in this sector of the Guadalquir paleoestuary comes from −12.5 m in the core S11, at which depth medium- to fine-grained sands containing abundant marine fauna have yielded a date of 5255–5461 cal yr BP (≈5300 cal yr BP) (Table 2 and Fig. 7). Slightly older dates have been obtained from other cores in the lower Guadalquivir river basin; for instance, the date 5617–5872 cal yr BP from the ML core (Zazo et al., 1999) and the date 5693–5910 cal yr BP from a core in the Carrizosa–Vetalarena ridge (Rodríguez-Ramírez et al., 2014). Following the Lower and Middle Holocene periods – when the study area was above sea level – Holocene formations have accumulated there since.

As the sea level inched upward, the Guadalquivir paleoestuary became very much open to the ocean. Sandy barriers began to develop and marine influence was high. The paleogeographical scenario must have been like that represented by Figure 8A. The corresponding macrofaunal and foraminifera assemblages indicate a brackish lagoon, with tidal flows introducing marine fauna toward the inner lagoonal areas. This model of the sedimentary infilling of the Guadalquivir paleoestuary accords with the results of comparable projects conducted in other estuaries of the Gulf of Cadiz (Lario et al., 1995; Dabrio et al., 2000; Boski et al., 2001). After ~5300 cal yr BP, the growth of the sandy barriers in the paleoestuary caused a number of silty–clayey formations to build up in an increasingly restricted environment. This gradual process of sedimentary infilling was then interrupted by several events of higher marine influence, which are described as follows.

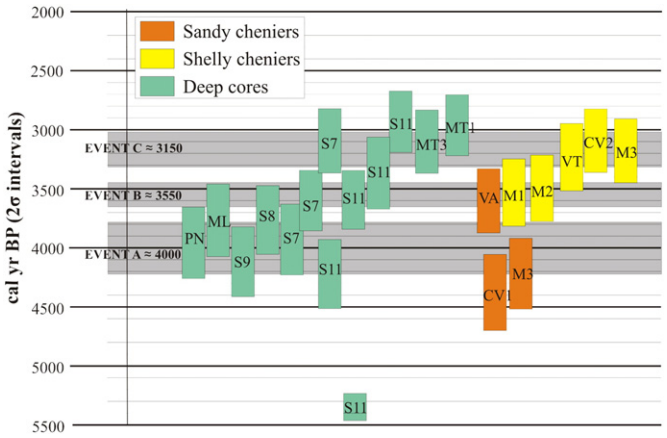

Figure 7. Graphical representation of dated samples (radiocarbon calibrated dataset) and different events (A, B, and C) over time during the Middle and Late Holocene. Rectangles indicate ranges of ^{14}C calibrated ages (cal.) with 2σ intervals. Orange rectangles refer to samples from sandy cheniers; yellow rectangles indicate samples from shelly cheniers; green applies to the deep boreholes.

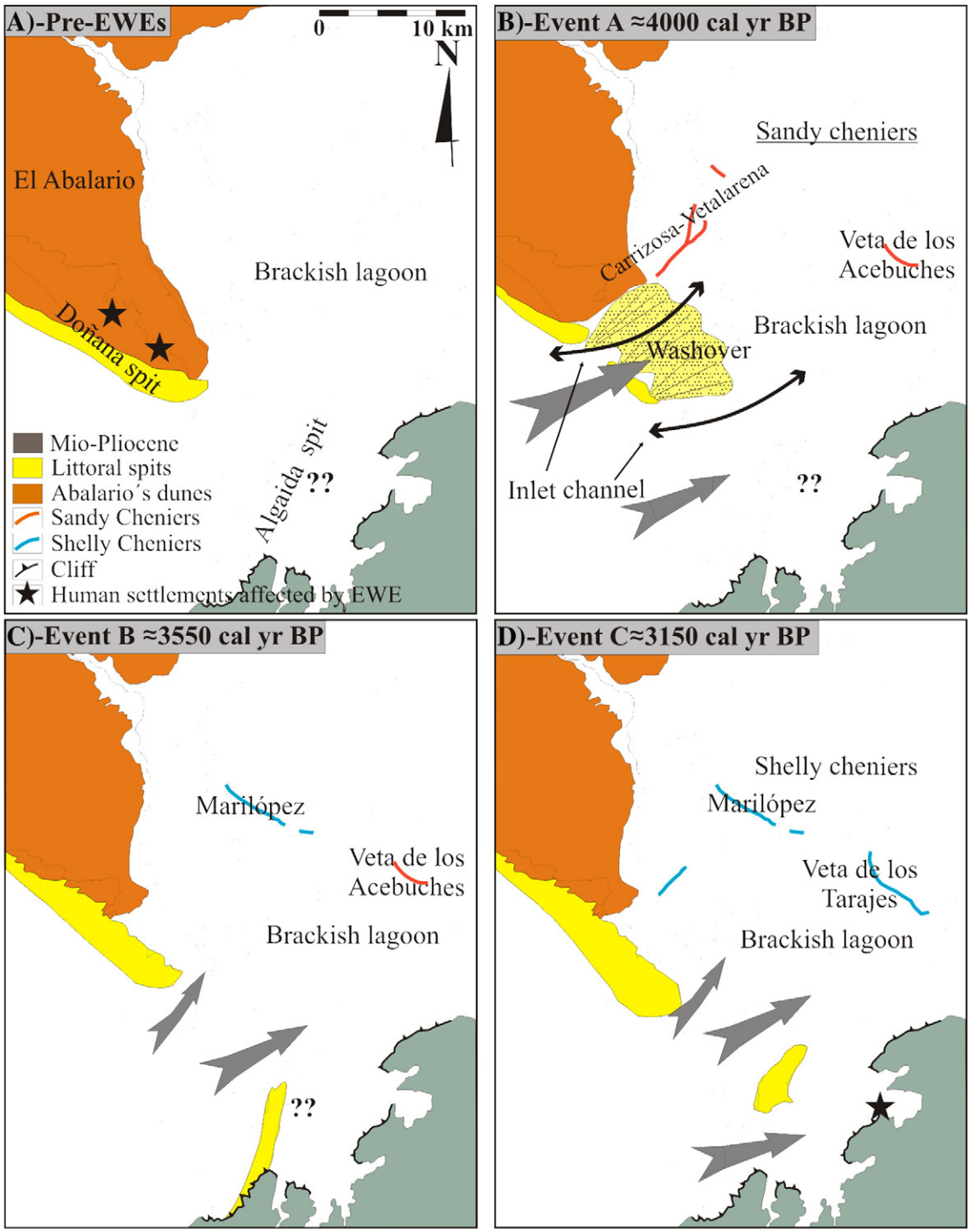

Figure 8. A. — Model of the paleogeographical scenario before the recognized EWEs. B. — Paleogeography during EWE A and post-event effects in the estuary (sandy cheniers). C. — Paleogeography during EWE B and post-event effects in the estuary (sandy cheniers in less confined areas (Veta de los Acebuches) and shelly cheniers in more confined areas (Marilópez). D. — Paleogeography during EWE C and post-event effects in the estuary (shelly cheniers).

The marine events

The deep as well as the surface cores analyzed register, in effect, a number of events of higher marine influence in the paleoestuary that present very characteristic facies (see Table 3). Lithostratigraphic, paleontological, and chronological evidence is rather significant for as many as three such marine incursions, which we have named "A," "B," and "C." The evidence is less significant for other events, to which we refer as "Minor Events." The three major occurrences were very likely favored by a sea-level relative rise in a context of sustained subsidence of the Doñana Spit from about 4000 to 2000 cal yr BP (Rodríguez-Ramírez et al., 2014) (Fig. 9C).

Event A

Evidence of this event appeared in core S7 at −8 m, in core S9 at −6 m, and in core S11 at −11.5 m. Such evidence consists of a sand layer that contains a massive accumulation of shells (both articulated and disarticulated bivalves) and shell fragments in a sandy–muddy matrix with gravel and lithoclasts, on an erosive base. The faunal composition is of a high, large diversity of species from different environments,

Table 3
Characteristics of the different events studied.

	S7	S11	MT3 and MT4	MT2 and MT1
Event C	Muddy matrix Alien lithoclasts Massive layer and erosive base Mixture of disarticulated valves, shell fragments and whole bivalves (estuarine) Moderate transport of benthic foraminifera and hyaline foraminifera High d/p ratio High diversity of species from different environments (mostly estuarine) Paleogeography: marginal area of a confined estuary behind a littoral barrier (Doñana Spit)	Silty sandy matrix Alien lithoclasts Fining-upwardly sequence and erosive base Mudpebbles Upper part of the succession shows bioturbation Mixture of disarticulated valves, shell fragments and whole bivalves (estuarine) Transported benthic foraminifera and porcelanaceous foraminifera High diversity of species from different environments (mostly estuarine) Paleogeography: central basin of a confined estuary behind a littoral barrier (Doñana Spit)	Sandy and sand-silty matrix Alien and large lithoclasts Massive layer and erosive base Mixture of disarticulated valves and shell fragments of marine environments Transported benthic foraminifera and relatively high P/B ratio High diversity of species dominated by estuarine forms Paleogeography: area of estuary exposed to marine dynamics by inlet channel	Mud-sandy matrix Mud pebbles Scarce lithoclasts Archeological remains Upper part of the succession shows bioturbation Low percentages of transported benthic foraminifera and P/B ratio dominated by estuarine forms. Mixture of estuarine and terrestrial (Gastropoda) species Paleogeography: area away from the coast and confined
Event B	Silty sandy Fining-upwardly successions Gradual contact whole shells (2 valves) and disarticulated valves Moderate transport of benthic foraminifera and hyaline foraminifera High P/B ratio and d/p ratio Moderated diversity of species, dominated by estuarine forms Paleogeography: lower-energy extreme wave event in a semiconfined estuary behind a littoral barrier (Doñana Spit)	Sandy silty matrix erosive base Decreasing grain-size sequences whole shells (2 valves) and disarticulated valves Transported benthic foraminifera and porcelanaceous foraminifera Moderated diversity of species of different environment Paleogeography: lower-energy extreme wave event in a semiconfined estuary behind a littoral barrier (Doñana Spit)	No data	No data
Event A	Heterometric sandy matrix Gravel and alien lithoclasts Massive layer and very erosive base Mixture of disarticulated valves, shell fragments and whole bivalves. Transported benthic foraminifera and porcelanaceous foraminifera High diversity of species dominated by open marine forms Paleogeography: breaking of littoral barrier by overwash and washover fan by large extreme wave event	Heterometric sandy and sandy silt matrix Lesser ratio of gravel and alien lithoclasts Wood Moderate fining-upward sequence and erosive base Moderate bioturbation Mixture of disarticulated valves, shell fragments and whole bivalves Transported benthic foraminifera and porcelanaceous foraminifera High diversity of species (mixture of marine and estuarine) Paleogeography: central basin of an open estuary	No data	No data

with predominance of open marine species and others that are typical of protected low-energy environments (Figs. 3, 4). In cores S7 and S9 this massive deposit sits erosively upon the aeolian El Abalario Dune Formation and the initial transgressive sands in the paleoestuary that we encountered in core S11. Core S11 is 3.5 km northeast of core S7 (Figs. 1 and 9). Subsequent sedimentation at S7 and S9 is characteristic of a submerged environment. The violent marine incursion probably affected the Neolithic and Copper Age human settlements that existed at the time in the area, as indicated by the artifacts found widely scattered among the dunes of El Abalario (Figs. 8A and B). The marine transgression must have destroyed at least some of these settlements and spread the remains across the estuarine basin. These remains later accumulated in sandy cheniers (as identified at CV1).

Revealing of its formation, such thick sandy deposit recognized in cores S7 and S9 presents morphostratigraphic features of a washover fan developed by an overwash process that broke the pre-existing sandy barrier (Fig. 9B) and formed a tidal channel that favored, after the event, the growth of the Carrizosa–Vetalarena sandy littoral strands toward the northeast (Fig. 8B). Such a process could account for the dominance of porcelanaceous benthic foraminifera, with more resistant shells, over the softer hyaline benthic foraminifera which may have been transported from very shallow environments and later reworked in the foreshore and the backshore. During this time, the barrier morphology was probably dominated by a low-relief ridge and swale topography (Fig. 9B) that invited greater marine influence and the formation of sandy cheniers.

A number of studies have described washover features as a product of high-energy events, discussing the possibility that such features may have sprung from tsunamis or strong storms (Switzer et al., 2004, 2005, 2006). In storm events, the washover facies appear in sites adjacent to former barrier islands, never in the inner parts of estuaries (Morton et al., 2007). In the lower Guadalquivir basin, the sand layer denoting Event A has been found to spread considerably toward the inner estuary (≈10 km), to points S11, PN, and ML, and perhaps farther in. This formation, therefore, has a wide distribution, extending both laterally and longitudinally over several kilometers. Depending upon the distance from the coastline, the formation presents different facies: at points S7 and S9, facies are more proximal and, therefore, coarser-grained, whereas at S11 they are intermediate and finer-grained. At the more distal PN, the facies offer a lithology dominated by a muddy–sandy layer and a mixture of open marine species and species characteristic of protected low-energy environments (Pozo et al., 2010). Furthermore, the thickness of the sandy layer in S7, S9, and S11 (40 to 70 cm) falls well within the thickness range (20–80 cm) concluded for many tsunamitic sandy deposits (Fujiwara et al., 2000; Nanayama et al., 2000; Bussert and Aberhan, 2004; Goff et al., 2004; Puga-Bernabéu et al., 2007; Goff et al., 2012; Smit et al., 2012).

Because of its morphostratigraphic size and its paleontological, lithological, and sedimentary contents, it is possible to establish an origin related to a high-energy event for this sandy layer. The proximal facies found in S7 and S9 can be included in Type 1 of the tsunamites described by Fujiwara et al. (2000), characterized by massive accumulation of high diversity of shells and shell fragments, alien lithoclasts, sandy matrix,

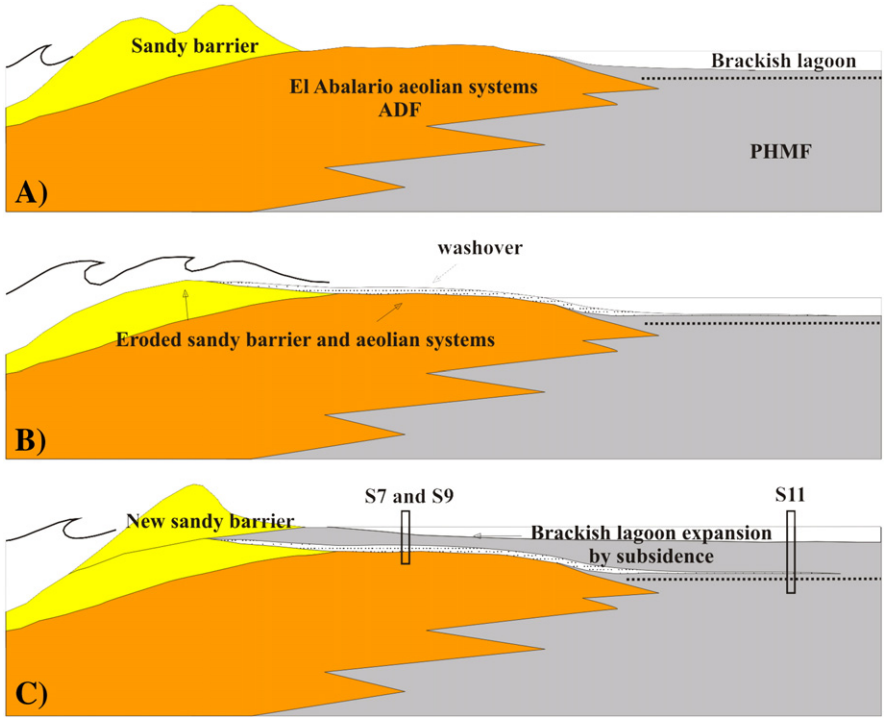

Figure 9. Schematic evolutionary diagram of an overwash process during EWE A. A. — Situation before the erosional event. B. — Overwash and severe erosion of sandy barrier and aeolian systems. C. — Sandy barrier reconstruction and Brackish lagoon expansion facilitated by subsidence processes.

and an erosive base. The intermediate facies at S11 may be regarded as fitting Type 2 in the same classification, characterized by fining-upwards successions, erosive base, sandy or sandy gravel ceiling with muddy matrix, shell accumulation from different environments, and an upper part of the succession usually showing bioturbation. The distal facies of PN could fall in Type 3, characterized by sandy–muddy layers with erosive bases, decreasing grain-size, and presence of marine microorganisms, especially diatoms (Sawai, 2002) and ostracods (Smoot et al., 2000).

The ^{14}C dates for this ocean-born formation are 3635–4231 cal yr BP in S7, 3832–4410 cal yr BP in S9, and 3931–4510 cal yr BP in S11 (Table 2 and Fig. 7). Reworking in the third sample (from S11) may have resulted in a slightly older age than the real one, however. Other studies based on analysis of deep cores from the lower Guadalquivir basin, such as PN (Pozo et al., 2010) and ML (Zazo et al., 1999), have produced evidence of the same event, to which similar approximate dates have been given: 3665–4269 cal yr BP in PN and 3473–4066 cal yr BP in ML. Additional evidence, in the form of an interbedded marine layer, has been encountered as far inland as the inner marsh deposits of the paleoestuary (Lario et al., 2001). Such marine layer may have been unknowingly detected farther inland still, near the northermost boundary of the paleoestuary, interrupting for a long time the formation of a delta at the original outlet of the Guadalquivir River (Arteaga et al., 1995). By taking into account all the different radiocarbon determinations obtained for this scattered evidence, it can be concluded that the event very probably occurred within the range 3800–4200 cal yr BP, the likely average date then being ~4000 cal yr BP. This event would have produced a great erosive phase in the development of at least the sandy barriers in the Guadalquivir estuary that had started within the range 4000–4500 cal yr BP, after the maximum marine transgression there (Rodríguez-Ramírez et al., 1996). The sequence of proximal, intermediate, and distal facies left in the analyzed cores, the extensive area of the paleoestuary affected by the event, and the great paleogeographical changes that the event unleashed, including a large overwash of the southernmost section of El Abalario, are all clear signs of a tsunamigenic process of large magnitude. These signs, however, have not been recognized elsewhere in the Gulf of Cadiz (Lario et al., 2010). Neither are turbidite deposits generated by a strong earthquake of this age that have been reported (Gràcia et al., 2010). Yet the ~4000 cal yr BP event had rather violent effects in the Guadalquivir estuary, probably in connection with intense subsidence detected in the area (Rodríguez-Ramírez et al., 2014). In order to find evidence of its impact in the other estuaries of the Gulf, further research is necessary there.

Event B

Cores S7 and S11 present a sandy–muddy layer at −5.5 m and −9 m, respectively, with erosive base with regard to the underlying silty formation. The accumulation of shells includes disarticulated valves and shell fragments from protected low-energy environments, with very scarce species from the open sea. The microfauna consist mostly of estuarine foraminifera, with a slight increase in dinoflagellates and relatively few marine transported foraminifera (Fig. 3). The dates obtained in these levels are 3347–3867 cal yr BP in S7 and 3352–3862 cal yr BP in S11. The probable average age appears to be ~3550 cal yr BP.

The sedimentological and faunal features of such sedimentary formation make it difficult to establish whether it was produced by a tsunami or by a storm surge; in some cases the sedimentological features of tsunamis and storm events have been found to exhibit similar textural, structural, and sedimentary properties (Morton et al., 2007; Jaffe et al., 2008). Yet turbidite deposits in the Southwest Portuguese Margin related to a seismic event occurring ~3600 cal yr BP have been reported by Vizcaíno et al. (2006); it is possible, therefore, to assign the second energetic formation found in S7 and S11 to a moderate seismic event that generated a local tsunami around that date. In any case, ~3550 cal yr BP this sector of the estuary was quite confined, due to the growth of the Doñana Spit (Fig. 8C). At point S7 the sedimentological record is very clear in this regard: marine inputs were lower at the time. At S11, located in a more central area of the paleoestuary, a different scenario obtains: the core drilled there shows higher marine influence. North of S11, the chenier plain contains shells and shell fragments related to such an energetic event (Rodríguez-Ramírez et al., 1996; Ruiz et al., 2005b; Rodríguez-Ramírez and Yáñez, 2008) (Fig. 8C).

Event C

Both the deep and surface cores register a third, more recent sedimentation event that is also peculiar: a muddy–sandy layer on an erosive base that contains an accumulation of shells and shell fragments, gravel, and lithoclasts. This sedimentation appeared at −2.5 m in S7 m and at −7 m in S11 (Fig. 2). In the latter core the layer consists of sandy silts (15–20% sand) in a fining-upward sequence that includes scattered small pebbles and mud pebbles. In S7 the sand content is slightly lower (5–10%), yet the shell accumulation is made of a mixture of articulated bivalves, disarticulated valves, and shell fragments; the species represented are many, from different environments. Consistently, the microfauna show slight increase in marine species, even though estuarine species predominate (Fig. 3). Cores MT3 and MT4, on the right bank of the Guadalquivir River, revealed a widespread sandy layer with gravel and large lithoclasts, as well as shell accumulation of different environments (marine and estuarine). In MT1 and MT2 the facies suggest a more restricted environment: a mud-sandy layer with erosive base and decreasing grain-size sequences that end with bioturbated muddy sediments. This kind of structures can also be observed in the tsunamite facies of the Tinto–Odiel estuary (Morales et al., 2008); some of the transported shells survived the transport and tried to escape up through the upper muddy sand layer, causing vertical burrows. The shell and microfauna accumulation is dominated by estuarine forms, even terrestrial forms (*Cochlicella* sp.).

Because of their chronology and their stratigraphic position, these deposits can be attributed to a single event that spread stratigraphically across the paleoestuary (Fig. 1) and adapted to its paleogeography (Fig. 8D). Their morphostratigraphic and paleontological features being similar to those of other formations studied elsewhere in the world (Fujiwara et al., 2000; Morales et al., 2008; Goff et al., 2012), they can be regarded as tsunamigenic, especially considering the distance of the relevant cores to the paleocoastline (10–15 km). In the Gulf of Cadiz a storm surge is not very likely to produce this type of sedimentary formation so far from the coast (Rodríguez-Ramírez et al., 2003). Furthermore, the facies obtained change significantly from the cores closer to the coast (MT3 and MT4) over to the cores that are distant from it (MT1 and S7). The facies at MT3 and MT4 recall Type 1 of tsunamites in the classification of Fujiwara et al. (2000): massive accumulation of shells, sandy matrix, gravel, lithoclasts, erosive base, high diversity of open marine species, and lateral continuity of the deposit. These are clear signs of tsunamis in an open coast oriented in the direction of the origin of the tsunami waves, where energy dissipation is lower and the waves can reach higher levels more efficiently (Fig. 8D). Where, on the contrary, the coast is more confined and, therefore, the energy of the wave is lower, as at MT1 and at S7, the result is a deposit with lower sand content, lower presence of marine fauna, and dominance of fauna from restricted environments – even fauna from the continent (gastropods) – as observed in tsunamites described by Morales et al. (2008) in the Tinto–Odiel estuary (Fig. 1). At MT3, by contrast, one finds large block deposits attached to the paleocliff, transported there from other areas with similar lithologies in front of the coastal system. These facies have been described in previous studies (Whelan and Kelletat, 2005; Gracia et al., 2006).

The different radiocarbon determinations procured from S7 (2826–3359 cal yr BP), S11 (3073–3669 cal yr BP), MT1 (2717–3203 cal yr BP), and MT3 (2858–3376 cal yr BP) make it possible to date this event ~3150 cal yr BP, within the range from 3000 to 3300 cal yr BP (Table 2 and Fig. 7). The energetic layer found in MT2 contained archeological remains from the Middle Bronze Age in SW Iberia, which ended ~1250 BC (~3250 BP) (Menanteau, 1979). Such archeological materials suggest that this event, like Event A, may have affected the human population settled by the Guadalquivir estuary (Fig. 8D). In addition, studies carried out in the estuaries of the Tinto–Odiel (Morales et al., 2008) and Guadalete rivers (see Fig. 1) (Lario et al., 1995; Dabrio et al., 1999; Luque et al., 2001) have identified a possible tsunami occurring in the Gulf of Cadiz ~3000 cal yr BP, which could well be the event to which we are here referring, Event C.

Minor events

These minor events would be related to slight sea-level fluctuations (±1 m) occurred during the maximum, or Flandrian, transgression of the Atlantic Ocean as well as to the influence of low-energy storms. In the Gulf of Cadiz the generation of storms follows a periodicity of 3 to 7 yr in connection with negative values of the NAO (North Atlantic Oscillation) index and a periodicity of 10 to 12 yr in possible connection with periods of less sunspot activity, which produce the most conspicuous storm surges (Rodríguez-Ramírez et al., 2003).

Confinement of the estuary

To judge from the faunal record on different cores (S7 and S11), the estuary in the study area became confined after Event C. Inputs of transported marine fauna decreased and both macrofauna and microfauna from sheltered environments became dominant (e.g., *H. germanica* assemblage) (Ruiz et al., 2005a; Murray, 2006; Pérez-Asensio and Aguirre, 2010) (Figs. 3, 4). The transition from an open estuary to a semi-closed estuary can be dated to ~3150 cal yr BP and could be related to coastal progradation and formation of sandy barriers in the river mouth. These littoral barriers are the emergent part of the Holocene highstand, which in the Atlantic–Mediterranean linkage area began to form by ~6500–7000 cal yr BP (Goy et al., 1986; Zazo et al., 1994; Dabrio et al., 2000). In the Guadalquivir estuary such confinement was gradual, as recorded by the successive littoral strands of the chenier plain (Rodríguez-Ramírez and Yáñez, 2008). The last remnant of the ancient brackish coastal lagoon, the so-called *Lacus ligustinus*, dates from the Roman and post-Roman periods (1st to 6th centuries AD). The fluvial dynamics and the generation of levees ended up isolating the estuary from any tidal influence some 500 yr ago (Rodríguez-Ramírez and Yáñez, 2008).

The analyzed cores do not show evidence of EWEs after ~3000 cal yr BP in the study area. Such evidence has been found in other estuaries of the Gulf of Cadiz, however (Morales et al., 2008; Lario et al., 2011). Traces of these later events might be found in more external locations of the Guadalquivir paleoestuary.

The chenier plain

A number of sandy littoral strands in the study area are part of the chenier plain that has formed in the lower Guadalquivir basin during the late Holocene (Rodríguez-Ramírez and Yáñez, 2008). While the Carrizosa–Vetalarena sandy littoral strands can be dated to 4071–4706 cal yr BP (at CV1) and 3922–4514 cal yr BP (at M3), the strands of Veta de los Acebuches (see Fig. 1) appear to be slightly more recent: 3334–3882 cal yr BP at VA point.

These sandy littoral strands, which contain shells from different environments, indicate an open estuary, not restricted by sandy barriers, up to at least 3300 cal yr BP. The progressive growth of the Doñana Spit toward the SE and the gradual closure of the tidal inlet would end up limiting the access of the Ocean to the sandy chenier of Carrizosa–Vetalarena, whereas the chenier of Veta de los Acebuches would have been longer exposed to direct marine influence, up to at least 3300 cal yr BP feeding off the sedimentary contributions made by the successive events occurring until then (Fig. 8C). Eventually, the infilling of the estuary rendered this chenier inactive and thereafter fossilized. The oldest evidence of exposed sedimentary units of the Guadalquivir estuary is thus the sandy littoral strands of Carrizosa–Vetalarena, which could mark the highlight of the relative sea-level rise reached during the Holocene in the Gulf of Cadiz.

The Guadalquivir chenier plain is the result of the reworking and subsequent deposit of the residual lag of sand, shells, pebbles, and archeological remains that had entered several kilometers far into paleoestuary by the energy of events of various kinds (storms, tsunamis, stream floods) in different ages, ending up accumulating in longshore bars or ridges (cheniers). For this reason it is not possible to determine

with certainty in the sandy and shelly cheniers whether the detrital elements encountered in them came from storms or tsunamis or had other sources (Augustinus, 1989; Rodríguez-Ramírez and Yáñez, 2008). While these energy events can be well identified in the cores drilled (S7, S11, ML, and PN), their traces appear mixed and reworked in the cheniers.

By contrast, the shelly littoral strands (at VT, M3, M1, M2, and CV2) suggest a partial closure of the estuary, as these cores reveal scant input of sand and presence of fauna from more restricted environments. The dates obtained (VT: 2966–3539 cal yr BP; M3: 2916–3464 cal yr BP; CV2: 2835–3369 cal yr BP; M2: 3210–3766 cal yr BP; M1: 3227–3808 cal yr BP) point to events that occurred between 3500 and 2900 cal yr BP, including Event B and Event C (Fig. 7). It is possible, however, that sandy cheniers form in areas that are more exposed to marine dynamics (Veta de los Acebuches) and shelly cheniers form in more confined areas (Marilópez) (Fig. 8C).

The accumulation processes in the shelly littoral strands are similar to those which take place in the sandy littoral strands. Because all these littoral strands work as sinks for all sediments entering the estuary, regardless of their marine or fluvial origin, the processes of mixing and reworking materials produced in the crests of them do not allow distinguishing the nature of the events that transported the sediments (Rodríguez-Ramírez and Yáñez, 2008). However, cheniers can provide information about estuarine dinamycs, relative sea levels, paleocoasts, and periods of estuary opening and closing.

Conclusions

This multidisciplinary study reveals at least three big extreme wave events in the Gulf of Cadiz in the 4th millennium BP. The first event (Event A), dated to about 4000 cal yr BP, impinged far and wide on the estuary. It included a washover fan which caused strong erosion in the Guadalquivir sandy barrier as well as in the aeolian systems of El Abalario, these and other significant paleogeographic changes probably affecting human settlements established in the area in the Neolithic period and the Copper Age (Figs. 7, 8). This event may have been strongly conditioned by the intense subsidence of the area. The second event (Event B) took place ~3550 cal yr BP, its impact on the estuary being of lesser magnitude than that of Event A. Its record can be correlated, at a regional level, with that of an earthquake ~3600 cal yr BP in the Southwest Portuguese Margin. The third event (Event C), ~3150 cal yr BP, covered an extensive geographic area and catastrophically affected a Middle Bronze Age settlement near the mouth of the Guadalquivir River. The record of this third event might be correlated with that of an event recognized in the Tinto–Odiel and Guadalete estuaries, also in the Gulf of Cadiz (Fig. 1).

Because of the large number of sites studied, the three events can be spatially correlated and the facies of their traces differentiated, from more proximal to more distal facies from the coastline. The most proximal are characterized by massive accumulation of shells and shell fragments in a sandy or sandy–muddy matrix, erosive base, highly diverse mixture of open marine species and species typical of protected low-energy environments, and exotic lithoclasts. The most distal facies present a muddy–sandy matrix, dominance of estuarine fauna, shell accumulation with a mixture of articulated–disarticulated bivalves and shell fragments, and even presence of continental species, mudpebbles, pebbles in a clayey matrix, and bioturbation in the upper muddy part of the sedimentary succession.

A progressive process of closure and infilling occurred in the Guadalquivir paleoestuary during the late Holocene. The transition from an open estuary scenario to a semi-closed one took place ~3150 cal yr BP, as a result of both the increase of coastal progradation and the growth of sandy barriers flanking the mouths of the river. The successive events described here punctuate the gradual isolation of the paleoestuary from the ocean, depositing ever finer facies and ever less allochthonous elements in the sedimentary record. At the time of Event C the old basin had become quite confined and, therefore, much impermeable to the actions of the open sea.

In relation to sea-level oscillation, the oldest evidence of exposed sedimentary units in the Guadalquivir estuary – and thereby a probable highlight of the relative sea level reached there in the Holocene – corresponds to the sandy littoral strands of Carrizosa–Vetalarena, ~4000–4500 cal yr BP.

Acknowledgments

We are indebted to a vast array of Spanish institutions: Fundación Caja de Madrid, Fundación Doñana 21, Ayuntamiento de Hinojos, Fundación FUHEM, Estación Biológica de Doñana (EBD), Espacio Natural de Doñana (END), Instituto Andaluz del Patrimonio Histórico (IAPH), Delegación de Cultura de la Junta de Andalucía in Huelva, and Organismo Autónomo Parques Nacionales del Ministerio de Medio Ambiente y Medio Rural y Marino. Without their encouragement and support, the Hinojos Project would never have sailed. The present paper is both a product of the Hinojos Project and a contribution to the IGCPs 526 ("Risks, resources, and record of the past on the continental shelf"), 567 ("Earthquake Archaeology and Palaeoseismology"), and 588 ("Preparing for coastal change"). Additional support by Junta de Andalucía to the Research Group RNM276 also is acknowledged. We thank reviewers and editors for their helpful comments. This is publication n° 60 from CEIMAR Publication Series.

References

Alonso, C., Gracia, F.J., Del Río, L., Anfuso, G., Benavente, J., Martínez, J.A., 2004. Registro morfosedimentario de eventos históricos de alta energía en el litoral atlántico del Estrecho de Gibraltar (Trafalgar–Tarifa). In: Benito, G., Díez Herrero, A. (Eds.), Contribuciones recientes sobre Geomorfología. SEG-CSIC, Madrid, pp. 263–271.

Andrade, C., 1992. Tsunami generated forms in the Algarve barrier islands. The Science of Tsunami Hazards 10, 21–33.

Andrade, C., Hindson, R., Freitas, C., Dawson, A., 1994. Sedimentary evidence of tsunami flooding in the Algarve coastal lowlands. Proceedings of the Symposium of the Littoral '94 (1). Eurocoast-Portugal Association, Lisbon, pp. 1035–1036.

Arteaga, O., Schulz, H.D., Roos, A.M., 1995. El problema del "*Lacus ligustinus*": investigaciones geo-arqueológicas en torno a las marismas del Bajo Guadalquivir. In: Ruiz Mata, D. (Ed.), Tartessos 25 años después, 1968–1993: Actas del Congreso Conmemorativo del V Symposium Internacional de Prehistoria Peninsular. Ayuntamiento de Jerez de la Frontera, Biblioteca de Urbanismo y Cultura, Jerez de la Frontera, pp. 99–133.

Augustinus, P.G.E.F., 1989. Cheniers and chenier plains: a general introduction. Marine Geology 90, 219–229.

Baptista, M.A., Miranda, J.M., 2009. Revision of the Portuguese catalog of tsunamis. Natural Hazards and Earth System Sciences 9, 25–42.

Baptista, M.A., Miranda, P.M.A., Mendes, V.L., 1998. Constraints on the source of the 1755 Lisbon tsunami inferred from numerical modelling of historical data. Journal of Geodynamics 25, 159–174.

Bermúdez, J.L., Peinado, M.D., 2005. El Riesgo de Tsunami en Andalucía. Spin Cero 9, 3–8.

Bondevik, S., Svendsen, J.I., Mangerud, J., 1997. Tsunami sedimentary facies deposited by the Storegga tsunami in shallow marine basins and coastal lakes, western Norway. Sedimentology 44, 1115–1131.

Borrego, J., Morales, J.A., Pendon, J.G., 1993. Holocene filling of an estuarine lagoon along the mesotidal coast of Huelva: the Piedras River mouth, southwestern Spain. Journal of Coastal Research 9, 242–254.

Boski, T., Moura, D., Veiga-Pires, C., Camacho, S., Duarte, D., Scott, D.B., Fernández, S.G., 2001. Postglacial sea-level rise and sedimentary response in the Guadiana Estuary, Portugal/Spain border. Sedimentary Geology 150, 103–121.

Bridge, J.S., 2008. Discussion of articles in "Sedimentary features of tsunami deposits". Sedimentary Geology 211 (3–4) (94 pp.).

Bussert, R., Aberhan, M., 2004. Storms and tsunamis: evidences of event sedimentation in the Late Jurassic Tendaguru beds of southeastern Tanzania. Journal of African Earth Sciences 39, 549–555.

Campos, M.L., 1992. El riesgo de tsunamis en España. Análisis y valoración geográficaMadrid: IGN Monografías. 9, (204 pp.).

Campos, J.M., Gómez-Toscano, F., 1997. La ocupación humana entre los tramos bajos del Guadiana y el Guadalquivir. Su incidencia en la costa holocena. In: Rodríguez-Vidal, J. (Ed.), Cuaternario ibérico. Huelva, AEQUA, pp. 305–313.

Cruse, K., 1979. A review of water well drilling methods. The Quarterly Journal of Engineering Geology 12, 79–95.

Cuena, G.J., 1991. Proyecto de regeneración de las playas de Isla Cristina. Informe del Servicio de Costas. Madrid: Ministerio de Obras Públicas y Turismo, 100 pp. Unpublished report.

Dabrio, C.J., Goy, J.L., Zazo, C., 1999. The record of the tsunami produced by the 1755 Lisbon earthquake in Valdelagrana spit (Gulf of Cadiz, southern Spain). Geogaceta 23, 31–34.

Dabrio, C.J., Zazo, C., Goy, J.L., Sierro, F.J., Borja, F., Lario, J., González, J.A., Flores, J.A., 2000. Depositional history of estuarine infill during the Late Pleistocene–Holocene postglacial transgression. Marine Geology 162, 381–404.
Dawson, S., Smith, D.E., 2000. The sedimentology of mid-Holocene tsunami facies in northern Scotland. Marine Geology 170, 69–79.
Dawson, A.G., Smith, D.E., Ruffman, A., Shi, S., 1996. The diatom biostratigraphy of tsunami sediments: examples from recent and middle Holocene events. Physics and Chemistry of the Earth 21, 87–92.
Foster, I.D.L., Albon, A.J., Bardell, K.M., Fletcher, J.L., Jardine, T.C., Mothers, R.J., Pritchard, M.A., Turner, S.E., 1991. High energy coastal sedimentary deposits: an evaluation of depositional processes in southwest England. Earth Surface Processes and Landforms 16, 341–356.
Fujiwara, O., Masuda, F., Sakai, T., Irizuki, T., Fuse, K., 2000. Tsunami deposits in Holocene bay mud in southern Kanto region, Pacific coast of central Japan. Sedimentary Geology 135, 219–223.
Galbis Rodríguez, J., 1932–1940. Catálogo sísmico de la zona comprendida entre los meridianos 5° E y 20° W de Greenwich y los paralelos 45° y 25° N, in 2 Vols. Dirección General del Instituto Geográfico, Catastral y de Estadística, Madrid, (1014 pp.).
Goff, J., McFadgen, B.G., Chagué-Goff, C., 2004. Sedimentary differences between the 2002 Easter storm and the 15th-century Okoropunga tsunami, southeastern North Island, New Zealand. Marine Geology 204, 235–250.
Goff, J., Chagué-Goff, C., Nichol, S., Jaffe, B., Dominey-Howes, D., 2012. Progress in palaeotsunami research. Sedimentary Geology 243–244, 70–88.
González-Regalado, M.L., Ruiz, F., Tosquella, J., Baceta, J.I., Pendón, J.G., Abad, M., Hernández-Molina, F.J., Somoza, L., Díaz del Río, V., 2001. Foraminíferos bentónicos actuales de la plataforma continental del norte del Golfo de Cádiz. Geogaceta 29, 61–64.
Goy, J.L., Zazo, C., Dabrio, C.J., Hillaire-Marcel, C., 1986. Évolution des systèmes de lagoons-îles barrière du Tyrrenien a l'actualité à Campo de Dalías (Almería, Espagne). Travaux et Documents. 197. Éditions de l'ORSTOM, Paris, pp. 169–171.
Gracia, F.J., Alonso, C., Benavente, J., Anfuso, G., Del Río, L., 2006. The different coastal records of the 1755 tsunami waves along the South Atlantic Spanish coast. Zeitschrift für Geomorphologie, Supplementbände 146, 195–220.
Gràcia, E., Vizcaíno, A., Escutia, C., Asioli, A., Rodés, A., Pallás, R., Garcia-Orellana, J., Lebreiro, S., Goldfinger, C., 2010. Holocene earthquake record offshore Portugal (SW Iberia): testing turbidite palaeoseismology in a slow-convergence margin. Quaternary Science Reviews 29 (9–10), 1156–1172.
Gutiérrez-Mas, J.M., Juan, C., Morales, J.A., 2009. Evidence of high-energy events in shelly layers interbedded in coastal Holocene sands in Cadiz Bay (south-west Spain). Earth Surface Processes and Landforms 34, 810–823.
Hughen, K.A., Baillie, M.G.L., Bard, E., Bayliss, A., Beck, J.W., Blackwell, P.G., Buck, C.E., Burr, G.S., Cutler, K.B., Damon, P.E., Edwards, R.L., Fairbanks, R.G., Friedrich, M., Guilderson, T.P., Herring, C., Kromer, B., McCormac, F.G., Manning, S.W., Ramsey, C.B., Reimer, P.J., Reimer, R.W., Remmele, S., Southon, J.R., Stuiver, M., Talamo, S., Taylor, F.W., van der Plicht, J., Weyhenmeyer, C.E., 2004. Marine04 Marine radiocarbon age calibration, 26–0 ka BP. Radiocarbon 46, 1059–1086.
Jaffe, B.E., Morton, R.A., Kortekaas, S., Dawson, A.G., Smith, D.E., Gelfenbaum, G., Foster, I.D. L., Long, D., Shi, S., 2008. Reply to J.S. Bridge, 2008, Discussion of articles in "Sedimentary features of tsunami deposits". Sedimentary Geology 211, 95–97.
Kortekaas, S., Dawson, A.G., 2007. Distinguishing tsunami and storm deposits: an example from Martinhal, SW Portugal. Sedimentary Geology 200, 208–221.
Lambeck, K., Yokoyama, Y., Purcell, T., 2002. Into and out of the last glacial maximum: sea-level change during oxygen isotope stages 3 and 2. Quaternary Science Reviews 21, 343–360.
Lario, J., Zazo, C., Dabrio, C.J., Somoza, L., Goy, J.L., Bardají, T., Borja, F., 1995. Record of recent Holocene sediment input on Spit Bars and Deltas of South Spain. Journal of Coastal Research 17, 241–245.
Lario, J., Zazo, C., Plater, A.J., Goy, J.L., Dabrio, C.J., Borja, F., Sierro, F.J., Luque, L., 2001. Particle size and magnetic properties of Holocene estuarine deposits from Doñana National Park (SW Iberia): evidence of gradual and abrupt coastal sedimentation. Zeitschrift für Geomorphologie 45, 33–54.
Lario, J., Luque, L., Zazo, C., Goy, J.L., Spencer, C., Cabero, A., Bardají, T., Borja, F., Dabrio, C.J., Civis, J., González-Delgado, J.A., Borja, C., Alonso-Azcárate, J., 2010. Tsunami vs. storm surge deposits: a review of the sedimentological and geomorphological records of extreme wave events (EWE) during the Holocene in the Gulf of Cadiz, Spain. Zeitschrift für Geomorphologie 54 (Suppl. 3), 301–316.
Lario, J., Zazo, C., Goy, J.L., Silva, P.G., Bardají, T., Cabero, A., Dabrio, C.J., 2011. Holocene palaeotsunami catalogue of SW Iberia. Quaternary International 242, 196–200.
Levret, A., 1991. The effects of the November 1, 1755 "Lisbon" earthquake in Morocco. Tectonophysics 193, 83–94.
Luque, L., Lario, J., Zazo, C., Goy, J.L., Dabrio, C.J., Silva, P.G., 2001. Tsunami deposits as palaeoseismic indicators: examples from the Spanish coast. Acta Geologica Hispánica 36, 197–211.
Luque, L., Lario, J., Civis, J., Silva, P.G., Zazo, C., Goy, J.L., Dabrio, C.J., 2002. Sedimentary record of a tsunami during Roman times, Bay of Cadiz (Spain). Journal of Quaternary Science 17, 623–631.
Martínez Solares, J.M., López Arroyo, A., Mezcua, J., 1979. Isoseismal map of the 1755 Lisbon earthquake obtained from Spanish data. Tectonophysics 53, 301–313.
Menanteau, L., 1979. Les Marismas du Guadalquivir: Exemple de transformation d'un paysage alluvial au cours du Quaternaire récent. (Thèse 3e cycle) Université de Paris-Sorbonne, Paris.
Mendes, I., González, R., Dias, J.M.A., Lobo, F., Martins, V., 2004. Factors influencing recent benthic foraminifera distribution on the Guadiana shelf (Southwestern Iberia). Marine Micropaleontology 51, 171–192.
Morales, J.A., Borrego, J., San Miguel, E.G., López-González, N., Carro, B., 2008. Sedimentary record of recent tsunamis in the Huelva Estuary (southwestern Spain). Quaternary Science Reviews 27, 734–746.
Morales, J.A., Gutiérrez-Mas, J., Borrego, J.M., Rodríguez-Ramírez, A., 2011. Sedimentary characteristics of the Holocene tsunamigenic deposits in the coastal systems of the Cadiz Gulf (Spain). In: Mörner, N.A. (Ed.), The tsunami threat: Research and technology, pp. 237–258.
Morton, R.A., Gelfenbaum, G., Jaffe, B.E., 2007. Physical criteria for distinguishing sandy tsunami and storm deposits using modern examples. Sedimentary Geology 200, 184–207.
Morton, R.A., Gelfenbaum, G., Buckley, M.L., Richmond, B.M., 2011. Geological effects and implications of the 2010 tsunami along the central coast of Chile. Sedimentary Geology 242 (1–4), 34–51.
Murray, J.W., 2006. Ecology and Applications of Benthic Foraminifera. Cambridge University Press, Cambridge, (426 pp.).
Nanayama, F., Shigeno, K., Satake, K., Shimokawa, K., Koitabashi, S., Miyasaka, S., Ishii, M., 2000. Sedimentary differences between the 1993 Hokkaido-Nansei-Oki tsunami and the 1959 Miyakojima typhoon at Taisei, southwestern Hokkaido, northern Japan. Sedimentary Geology 135, 255–264.
Pérez-Asensio, J.N., Aguirre, J., 2010. Benthic foraminiferal assemblages in temperate coral-bearing deposits from the Late Pliocene. Journal of Foraminiferal Research 40, 61–78.
Pozo, M., Ruiz, F., Carretero, M.I., Rodríguez-Vidal, J., Cáceres, L.M., Abad, M., González-Regalado, M.L., 2010. Mineralogical assemblages, geochemistry and fossil associations of Pleistocene–Holocene complex siliciclastic deposits from the Southwestern Doñana National Park (SW Spain): a palaeoenvironmental approach. Sedimentary Geology 225, 1–18.
Puga-Bernabéu, Á., Martín, J.M., Braga, J.C., 2007. Tsunami-related deposits in temperate carbonate ramps, Sorbas Basin, southern Spain. Sedimentary Geology 199, 107–127.
Ramírez-Herrera, M.T., Lagos, M., Hutchinson, I., Kostoglodov, V., Machain, M.L., Caballero, M., Goguitchaichvili, A., Aguilar, B., Chagué-Goff, C., Goff, J., Ruiz-Fernández, A.C., Ortiz, M., Nava, H., Bautista, F., Lopez, G.I., Quintana, P., 2012. Extreme wave deposits on the Pacific coast of Mexico: tsunamis or storms? Geomorphology 139–140, 360–371.
Rodríguez-Ramírez, A., 2009. Discussion of the paper "The Geological record of the oldest historical tsunamis in southwestern Spain," by Ruiz, F., Abad, M., Rodríguez-Vidal, J., Cáceres, L.M., González-Rgalado, M.G., Carretero, M.I., Pozo, M., Gómez-Toscano, F., in Rivista Italiana di Paleontología e Stratigrafía, 2008, 114 (1): 147–156. Rivista Italiana di Paleontologia e Stratigrafia 115 (1), 133–134.
Rodríguez-Ramírez, A., Yáñez, C.M., 2008. Formation of chenier plain of the Doñana marshland (SW Spain): observations and geomorphic model. Marine Geology 254, 187–196.
Rodríguez-Ramírez, A., Rodríguez-Vidal, J., Cáceres, L., Clemente, L., Belluomini, G., Manfra, L., Improta, S., de Andrés, J.R., 1996. Recent coastal evolution of Doñana National Park (Southern Spain). Quaternary Science Reviews 15, 803–809.
Rodríguez-Ramírez, A., Ruiz, F., Cáceres, L.M., Rodríguez-Vidal, J., Pino, R., Muñoz, J.M., 2003. Analysis of the recent storm record in the south-western Spain coast: implications for littoral management. The Science of the Total Environment 303, 189–201.
Rodríguez-Ramírez, A., Flores, E., Contreras, C., Villarías-Robles, J.J.R., Jiménez-Moreno, G., Pérez-Asensio, J.N., López-Sáez, J.A., Celestino-Pérez, S., Cerrillo-Cuenca, E., León, A., 2014. The role of neo-tectonics in the sedimentary infilling and geomorphological evolution of the Guadalquivir estuary (Gulf of Cadiz, SW Spain) during the Holocene. Geomorphology 219, 126–140.
Ruiz, F., González-Regalado, M.L., Pendón, J.G., Abad, M., Olías, M., Muñoz, J.M., 2005a. Correlation between foraminifera and sedimentary environments in recent estuaries of southwestern Spain: applications to Holocene reconstructions. Quaternary International 140–141, 21–36.
Ruiz, F., Rodríguez-Ramírez, A., Cáceres, L.M., Rodríguez-Vidal, J., Carretero, M.I., Abad, M., Olías, M., Pozo, M., 2005b. Evidence of high-energy events in the geological record: mid-Holocene evolution of the southwestern Doñana National Park (SW Spain). Palaeogeography, Palaeoclimatology, Palaeoecology 229, 212–229.
Salvany, J.M., Larrasoaña, J.C., Mediavilla, C., Rebollo, A., 2011. Chronology and tectono-sedimentary evolution of the Upper Pliocene to Quaternary deposits of the lower Guadalquivir foreland basin, SW Spain. Sedimentary Geology 241, 22–39.
Sawai, Y., 2002. Evidence for 17th-century tsunamis generated on the Kuril–Kamchatka subduction zone, Lake Tokotan, Hokkaido, Japan. Journal of Asian Earth Sciences 20, 903–911.
Scheffers, A., Kelletat, D., 2005. Tsunami relicts on the coastal landscape west of Lisbon, Portugal. Science of Tsunami Hazards 23, 3–16.
Smit, J., Laffra, C., Meulenaars, K., Montanari, A., 2012. Probable late Messinian tsunamiites near Monte Dei Corvi, Italy, and the Nijar Basin, Spain: expected architecture of offshore tsunami deposits. Natural Hazards 63, 241–266.
Smoot, J., Litwin, R., Bischoff, J., Lund, S., 2000. Sedimentary record of the 1872 earthquake and Tsunami at Owens Lake, southeast California. Sedimentary Geology 135 (1–4), 241–254.
Soares, A.M.M., Martins, J.M.M., 2010. Radiocarbon dating of marine samples from Gulf of Cadiz: the reservoir effect. Quaternary International 221, 9–12.
Stuiver, M., Reimer, P.J., 1993. Radiocarbon calibration program. Rev.4.2. Radiocarbon 35, 215–230.
Stuivert, M., Reimer, P.J., Bard, E., Beck, J.W., Burr, G.S., Hughen, K.A., Kromer, B., McCormac, F.G., van der Plicht, J., Spurk, M., 1998. INTCAL98 radiocarbon age calibration, 24,000–0 cal BP. Radiocarbon 40, 1041–1083.
Switzer, A.D., 2008. Twenty years of palaeotsunami studies on coastal sandsheets: a review. 2nd International Tsunami Field Symposium, IGCP Project 495. GI2S Coast Research Publication. 6, pp. 163–165.
Switzer, A.D., Jones, B.G., 2008. Large-scale washover sedimentation in a freshwater lagoon from the southeast Australian coast: sea-level change, tsunami or exceptionally large storm? The Holocene 18 (5), 787–803.
Switzer, A.D., Jones, B.G., Bristow, C.S., 2004. Geological evidence for large-scale washover events from coastal New South Wales, Australia: implications for management.

Delivering Sustainable Coasts: Connecting Science and Policy, Littoral 2004Proceedings. 1. Cambridge Publications, Brookline, MA, pp. 390–395.
Switzer, A.D., Pucillo, K., Haredy, R.A., Jones, B.G., Bryant, E.A., 2005. Sea level, storm or tsunami: enigmatic sand sheet deposits in a sheltered coastal embayment from southeastern New South Wales, Australia. Journal of Coastal Research 21 (4), 655–663.
Switzer, A.D., Bristow, C.S., Jones, B.G., 2006. An erosional signature for large-scale washover identified using ground penetrating radar on a small Holocene barrier from the southeast Australian coast. Sedimentary Geology 183, 145–146.
Terrinha, P., Pinheiro, L.M., Henriet, J.P., Matias, L., Ivanov, M.K., Monteiro, J.H., Akhmetzhanov, A., Volkonskaya, A., Cunha, T., Shaskin, P., Rovere, M., 2003. Tsunamigenic–seismogenic structures, neotectonics, sedimentary processes and slope instability on the southwest Portuguese Margin. Marine Geology 195, 55–73.
Vanney, J.R., 1970. L'hydrologie du Bas Guadalquivir. CSIC, Departamento de Geografía Aplicada, Madrid, (176 pp.).
Vizcaíno, A., Gràcia, E., Pallàs, R., Garcia-Orellana, J., Escutia, C., Casas, D., Willmott, V., Diez, S., Asioli, A., Dañobeitia, J.J., 2006. Sedimentology, physical properties and ages of mass-transport deposits associated to the Marquês de Pombal Fault, Southwest Portuguese Margin. Norwegian Journal of Geology 86, 177–186.
Whelan, F., Kelletat, D., 2003. Analysis of tsunami deposits at Cabo de Trafalgar, Spain, using GIS and GPS technology. Essener Geographische Arbeiten 35, 11–25.
Whelan, F., Kelletat, D., 2005. Boulder deposits on the southern Spanish Atlantic coast: possible evidence for the 1755 AD Lisbon tsunami? Science of Tsunami Hazards 23 (3), 25–38.
Zazo, C., Goy, J.L., Somoza, L., Dabrio, C.J., Belluomini, G., Improta, S., Lario, J., Bardají, T., Silva, P.G., 1994. Holocene sequence of relative sea level highstand–lowstand in relation to the climatic trends in the Atlantic–Mediterranean linkage coast: forecast for future coastal changes and hazards. Journal of Coastal Research 10 (4), 933–945.
Zazo, C., Dabrio, C.J., González, J., Sierro, F., Yll, E.I., Goy, J.L., Luque, L., Pantaleón-Cano, J., Soler, V., Roure, J.M., Lario, J., Hoyos, M., Borja, F., 1999. The records of the later glacial and interglacial periods in the Guadalquivir marshlands (Marilópez drilling, SW Spain). Geogaceta 26, 119–122.
Zazo, C., Mercier, N., Silva, P.G., Dabrio, C.J., Goy, J.L., Roquero, E., Soler, V., Borja, F., Lario, J., Polo, D., Luque, L., 2005. Landscape evolution and geodynamic controls in the Gulf of Cadiz (Huelva coast, SW Spain) during the Late Quaternary. Geomorphology 68, 269–290.
Zazo, C., Dabrio, C.J., Goy, J.L., Lario, J., Cabero, A., Silva, P.G., Bardají, T., Mercier, N., Borja, F., Roquero, E., 2008. The coastal archives of the last 15 ka in the Atlantic–Mediterranean Spanish linkage area: sea level and climatic changes. Quaternary International 181, 72–87.